

Dual-Electrolyte System for Suppressing Corrosion of Aluminum electrode in Aluminum-
Air Flow Battery



A Thesis Submitted in Partial Fulfillment of the Requirements
for the Degree of Master of Engineering in Chemical Engineering

Department of Chemical Engineering

Faculty of Engineering

Chulalongkorn University

Academic Year 2018

Copyright of Chulalongkorn University

ระบบอิเล็กทรอนิกส์เพื่อลดการกักตัวของไข้หวัดใหญ่ในแบตเตอรี่ลิเธียม-อากาศ
แบบไหล



วิทยานิพนธ์นี้เป็นส่วนหนึ่งของการศึกษาตามหลักสูตรปริญญาวิศวกรรมศาสตรมหาบัณฑิต
สาขาวิชาวิศวกรรมเคมี ภาควิชาวิศวกรรมเคมี
คณะวิศวกรรมศาสตร์ จุฬาลงกรณ์มหาวิทยาลัย
ปีการศึกษา 2561
ลิขสิทธิ์ของจุฬาลงกรณ์มหาวิทยาลัย

Thesis Title	Dual- Electrolyte System for Suppressing Corrosion of Aluminum electrode in Aluminum-Air Flow Battery
By	Miss Pemika Teabnamang
Field of Study	Chemical Engineering
Thesis Advisor	Associate Professor Soorathep Kheawhom, Ph.D.

Accepted by the Faculty of Engineering, Chulalongkorn University in Partial Fulfillment of the Requirement for the Master of Engineering

..... Dean of the Faculty of Engineering
(Associate Professor Supot Teachavorasinskun, D.Eng.)

THESIS COMMITTEE

..... Chairman
(Associate Professor Anongnat Somwangthanaroj, Ph.D.)

..... Thesis Advisor
(Associate Professor Soorathep Kheawhom, Ph.D.)

..... Examiner
(Pimporn Ponpesh, Ph.D.)

..... External Examiner
(Assistant Professor Pornchai Bumroongsri, D.Eng.)

ACKNOWLEDGEMENTS

First of all, I would like to show my appreciation to my thesis advisor, Assoc. Prof. Soorathep Kheawhom, for his advice and support throughout my graduate course. His suggestions have significantly improved my work and research insight. Without his assistance, the completion of this work would not have been possible.

I also gratefully acknowledge Assoc. Prof. Anongnat Somwangthanaroj, Ph.D. Pimporn Ponpesh, and Asst. Prof. Pornchai Bumroongsri who are the thesis committee members for their comments and recommendations. I want to thank the staff of the Department of Chemical Engineering who have assisted me in my work, especially Mr.Kijchai Karnkajanaprapakul. He has been most helpful in providing the technical assistance necessary for my experiment.

I would like to thank my father and mother for everything they have given to me. Without their love and support, my life would not come this far.

I want to thank my friends from process control and life cycle who were most supportive while I was studying for my Master's Degree. My friends from engineering have played an essential role in my graduate pursuits sharing their knowledge and encouraging me when I needed it the most.

My thanks also to Mr. J. Alan Wilcox, M.Ed., who helped me in the revision of my thesis.

Finally, I would like to show my gratefulness to Mr. Jetsada Sae-Chueng who always supported me.

จุฬาลงกรณ์มหาวิทยาลัย
CHULALONGKORN UNIVERSITY

Pemika Teabnamang

TABLE OF CONTENTS

	Page
ABSTRACT (THAI)	iii
ABSTRACT (ENGLISH).....	iv
ACKNOWLEDGEMENTS.....	v
TABLE OF CONTENTS	vi
Chapter 1	1
Introduction.....	1
1.1 Background	1
1.2 Objective	3
1.3 Scope of research	3
1.4 Schedule plan	5
Chapter 2	6
Theory	6
2.1 Theory	6
2.1.1 Aluminum-air batteries.....	6
2.1.2 The Air cathode	8
2.1.3 Electrolytes	10
2.1.4 Ion exchange membranes	11
2.1.5 Battery performance evaluation and effect of parameters.....	11
2.1.5.1 Open Circuit Voltage (OCV)	12
2.1.5.2 Polarization curve and overpotential	12
2.1.5.3 Power density	13

2.1.5.4 Specific capacity (S.C.).....	13
2.1.6 Corrosion and mechanism of aluminum in electrolyte.....	14
2.1.6.1 Tafel polarization	16
Chapter 3	18
Literature review	18
3.1 Literature review of the behavior of aluminum's corrosion	18
3.2 Literature of an aluminum-air battery	19
3.3 Literature of dual-electrolytes, flow system and other types of battery	22
Chapter 4	28
Methodology	28
4.1 Material and chemicals	28
4.2 Hydrogen evolution test.....	28
4.3 Half-cell test.....	29
4.4 Full cell test	30
Chapter 5	32
Results and discussion	32
5.1 The aluminum's corrosion in 3M KOH with anhydrous methanol, employing different percentage of deionized water, was investigated.	32
5.1.1 Hydrogen evolution	32
5.1.2 Tafel polarization.....	35
5.1.3 Electrochemical impedance spectroscopy (EIS).....	37
5.2 Battery performance.....	42
5.2.1 Effect of deionized water in the polarization of the I-V curve and power density	42
5.2.2 Effect of deionized water in discharge profile	45

5.2.3 Effect of flow rate with anhydrous methanol based electrolyte	50
Chapter 6	52
Conclusions	52
Appendix	54
REFERENCES	56
VITA	60



Chapter 1

Introduction

1.1 Background

Recently, climate change has become increasingly significant putting considerable pressure on various aspects of our environment. Thus, a sustainable solution for energy generation and storage needs to be actively developed. The aim of the energy field consists of proposing reliable power production and storage systems while ensuring a low environmental footprint. Nevertheless, the utilization and development of renewable energy systems are far from adequate. Consequently, governmental authorities worldwide aim to promote a renewable solution for electricity generation and storage.

According to the 4.0 energy policy of the Ministry of Energy of Thailand, consumption for electricity generation is 22% while natural gas accounts for 64%. Though several Renewable Energy Sources (RESs) are available, their contribution is only 6%. By 2036, the Government of Thailand aims to diversify electricity generation by boosting the proportion of RESs to 20% and reducing that of natural gas to 37%.

Electrical energy storage (EES) systems are essential for the effective utilization and integration of RESs to the grid. EES systems offer many benefits including improving the way energy is delivered, consumed and generated. Besides, EESs are expected to become increasingly common given the growing importance of the distributed generation of RESs. The most common kind of EES is the use of a battery. Lithium-ion batteries (LIBs) have been the most widely recognized EES devices employed in various applications. Unfortunately, the high cost and safety issues of Li-ion batteries are the primary barrier to their successful implementation. Further, Lithium (Li) supply, as well as its future production, are not sufficient for use in large-scale EES systems. Again, the distribution of Li is limited. A significant quantity of Li is found only in the Andes and Tibet. However, there are other mature technologies based on Nickel (Ni) such as nickel–metal hydride (NiMH) and Sodium Nickel Chloride (NaNiCl) batteries. Yet, Ni is also expensive and produced in relatively

limited quantities. Hence, these technologies will become affected by their Ni requirements for production in large quantities.

It is worth noting that Al-air batteries have high potential for future energy storage applications. Al-air batteries have a high specific capacity of 2.98 Ah/g which is the second highest after that of a Li-air battery (3.86 Ah/g) and much higher than a zinc-air battery (0.82 Ah/g). Furthermore, an aluminum anode is an inexpensive, abundant and environmentally friendly metal with high recyclability (Liu et al., 2017a). However, self-corrosion of the aluminum anode is a critical test for traditional Al/air batteries. Anodic corrosion results in the accumulation of hydrogen gas in the cell and increases the hydrogen explosion possibility. Besides, it causes unacceptably high energy losses.

Various works have attempted to inhibit aluminum self-corrosion by alloying aluminum with other elements or modifying the electrolyte using certain additives. Nevertheless, these efforts have shown limited success and have often increased the complexity of the battery system. To address this issue, aluminum oxidation should take place in a non-aqueous environment with high aluminum anode activity while suppressing the corrosion rate. Other approaches, which include employing gel electrolytes or ionic liquids, have also been introduced to address this problem.

Methanol (CH_3OH) was used as the electrolyte (L. Wang et al., 2014). Methanol was seen to provide a high capacity under a dual-electrolyte system in an Al-air battery whereby a non-aqueous electrolyte was used for the anolyte and an aqueous electrolyte was used for the catholyte. In the cathode, platinum-carbon (Pt-C) being a perfect gas diffusion electrode was used but it proved to be of high cost. However, anode passivation was not solved. Hence, this work proposes a dual-electrolyte Al/air cell with a structure of an Al anode | methanol electrolyte || gel polymer electrolyte | air cathode as well as a flow electrolyte which is used for solving the passivation problem. The air cathode used employs a standard recipe having carbon powder along with manganese dioxide for the catalyst. Thus, hydrogen evolution reaction can be suppressed, and a very high cell capacity can be achieved. The performance of the battery was then examined.

1.2 Objective

- 1) To investigate the behavior of self-corrosion of the aluminum electrode in organic and aqueous-organic electrolytes.
- 2) To investigate the performance of an Al-air flow battery using the dual-electrolyte system with organic and aqueous-organic electrolytes.

1.3 Scope of research

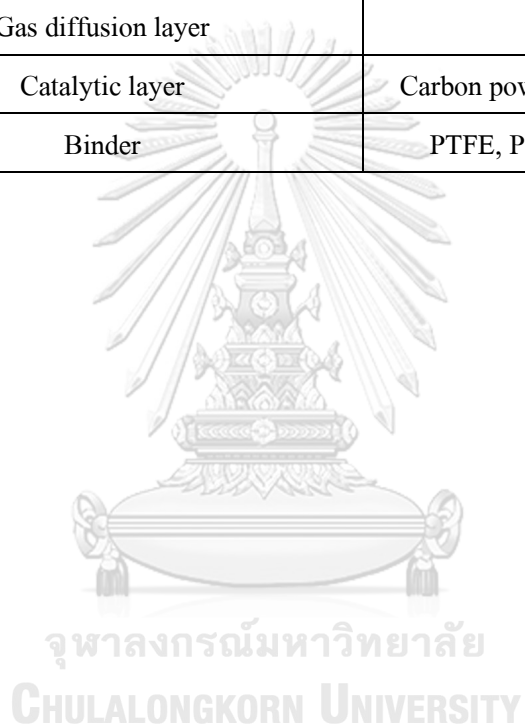
- 1) The homemade design of the battery's fabrication and components are shown in Tables 1.1 and 1.2.
- 2) Solvents used in the experiment were methanol and deionized water.
- 3) The concentration was 3M KOH and deionized water was added i.e. (0, 5, 10 and 20) %wt.
- 4) The studied parameter of feed flow rate was fixed at 40 rpm; the experiment was carried out at room temperature.
- 5) Electrochemical analysis was tested by VersaStudio software which employed Electrochemical Impedance Spectroscopy (EIS) and Tafel Polarization.
- 6) The performance of the battery was tested by Battery metric (MC2020 series) BA500WIN program studying current-voltage polarization and constant-current discharge.

Table 1.1 design equipment

Equipment	Dimension
Acyclic for anolyte WW*LL*HH	15*100*90
Acyclic for catholyte WW*LL*HH	5**100*90
Tube I.D.	10

Table 1.2 components

Component	Material
Separator	Anion exchange membrane
Anode	Aluminum plate pure 99.99%
Anolyte	Organic electrolyte
Catholyte	Gel polymer electrolyte
Cathode	Oxygen from air
Gas diffusion layer	Nickel foam
Catalytic layer	Carbon powder and manganese dioxide
Binder	PTFE, Poly(styrene-co-butadiene)



Chapter 2

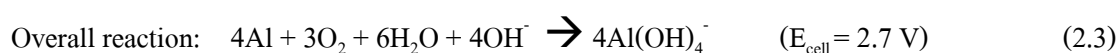
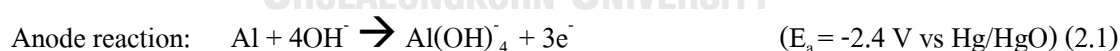
Theory

2.1 Theory

2.1.1 Aluminum-air batteries

A metal-air battery consists of metal for the anode, oxygen for the cathode and a suitable electrolyte. The oxygen adsorbed from the air passes through the cathode layer. The types of electrolyte used were as follows: sodium hydroxide (NaOH), potassium hydroxide (KOH) or sodium chloride (NaCl) solutions.

Aluminum is the one of the metals used in the anode's fuel cell. The open circuit potential of aluminum is positive at -1.66V vs. Hg/HgO since the electrode process takes place on the aluminum surface: namely (i) formation and dissolution of an initial Al₂O₃ and subsequent Al(OH)₃ layer (ii) three-electron charge transfer yielding Al of three species (iii) formation of corrosion production such as Al(OH)₃ (iv) a parasitic corrosion reaction involving the reduction of water at localized cathodic centres on the aluminum surface, which releases hydrogen (Egan et al., 2013). The Al-air battery has a high theoretical voltage around 2.7 V and its energy density is 8.1 kWh/kg. The normal form of an Al-air battery depends on the type of electrolyte that participates in the reaction. The electrochemical reaction based on hydroxide can be signified as follows (Liu et al., 2017b):



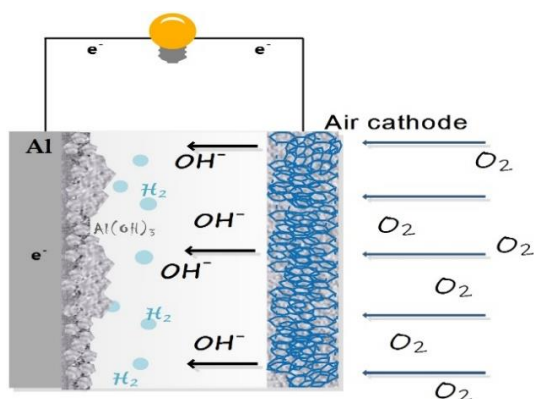


Figure 2.1 schematic diagram of an Aluminum-air Battery

A negative electrode involves the oxidation of aluminum which provides aluminum ions resulting in anode reaction. As for the cathode reaction, the positive electrode is an air or gas diffusion electrode having a carbon-based structure which adsorbs oxygen and brings the electrolyte into contact with a catalyst resulting in oxygen reduction (Egan et al., 2013).

Q. Li & Bjerrum (2002) stated that an aluminum anode has a half-cell potential of -2.4 V in an alkaline electrolyte and is of high potential. Normally, when an aluminum anode is immersed in an electrolyte corrosion reaction occurs. The corrosion reaction of aluminum provides a protective oxide film which amounts to passivation on the aluminum surface. Hence, when an aluminum electrode is saturated with aluminate, the aluminate concentration exceeds super-saturation. Thus, crystalline from aluminum hydroxide precipitates causing the regeneration of hydroxide ions. Thereby, parasitic hydrogen generation reaction takes place at the anode. The parasitic reaction can be expressed as follows:



The performance of an electrochemical cell is usually expressed in terms of a polarization curve. As shown in Fig. 2.2, the polarization curve indicates the behavior of cell potential in the function of current density. The polarization curve generally can be divided into 3 zones. The first zone is the activation loss zone. This zone ranges from OCV to the initial steep of potential decrease. The OCV is the electrical potential difference of an electrochemical cell. Activation losses are losses from slowness of the reactions. These losses dominate the first zone of the polarization curve. The second zone is the ohmic loss zone where the voltage slowly

decreases and is dominated by losses from electrical resistance of the cell components (electrodes and interconnection parts) and the resistance to the flow of ions in the electrolyte. The third zone is the concentration loss zone. This loss occurs at high current density due to mass transport limitation resulting in a rapid decrease in voltage.

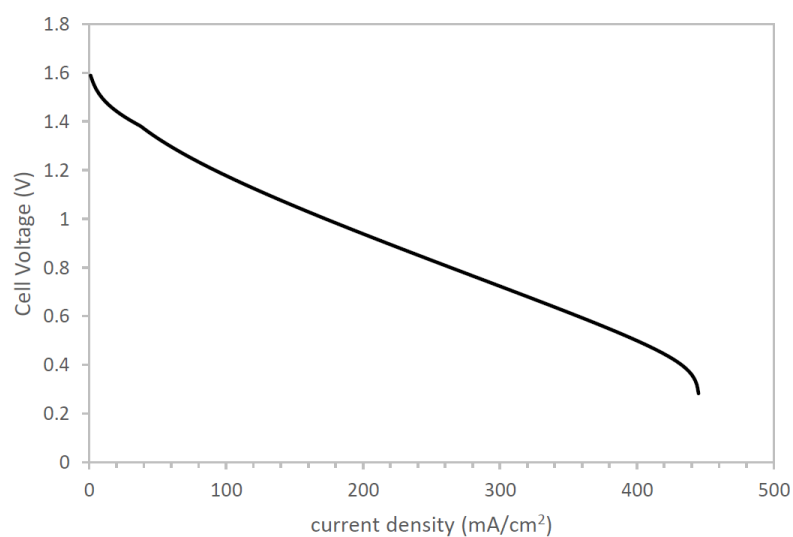


Figure 2.2 polarization curve of the battery

2.1.2 The Air cathode

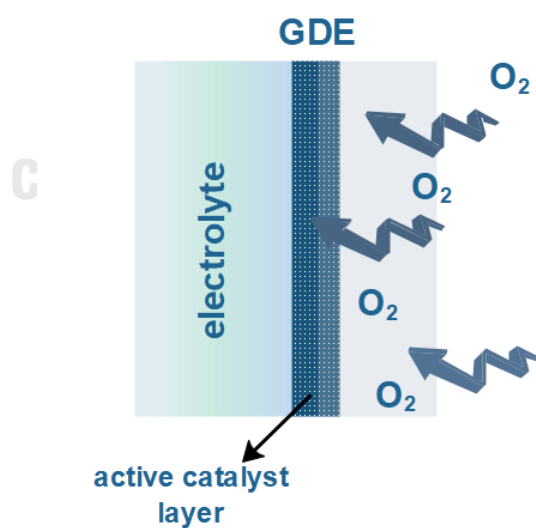


Figure 2.3 the structure of air diffuses into cathode pore at the hydrophobic layer and electrolyte attaches with catalyst active layer at the hydrophilic layer.

An air electrode always consists of a gas diffusion layer (GDL), a current collector and an active catalyst layer improving the performance of the battery. The gas diffusion layer is made up of carbon material and a hydrophobic binder such as polytetrafluoroethylene (PTFE) or poly(styrene-co-butadiene). The current collector is usually made of nickel metal that can be connected to the external circuit and can increase the electron transfer process. The active catalytic layer brings about the consumption of oxygen reduction reaction (ORR). The oxygen from the air reacts at the cathode; thus, oxygen is reduced via electrons together with water and is transformed into hydroxide ions. The electrode is prepared using carbon conductive additive as a binder and is coated on the electrode plate (Mokhtar et al., 2015). The oxygen reduction reaction (ORR) and oxygen reduction catalyst must be combined with the composite electrode to catalyze the ORR to support the composite electrode effectively. Table 2.1 shows the problems found (Liu et al., 2017a).

Table 2.1 Problems of the air electrode, cause and solutions

Problems	cause	Effect	Proposed solutions
Inert oxygen reaction	High potential required for driving ORR and OER	Limited energy/power density and energy efficiency	Explore efficient, durable electrocatalysts
Air electrode flooding	Electrolyte penetration into the pores of the air cathode	Reduced oxygen accessibility	Treat carbon electrode with wax or proper optimization of GDL
Carbonate precipitation	CO ₂ reacts with alkaline electrolyte then produce carbonate	Decreased electrolyte conductivity and air cathode activity	Supply pure O ₂ to reduce the CO ₂ concentration
Electrolyte drying out	Water evaporation to open air	Battery life reduced	Proper optimization of GDL

2.1.3 Electrolytes

The performance of metal-air batteries depends on selecting a suitable electrolyte system. An acidic electrolyte produces a large volume of hydrogen as well as a huge amount of heat which causes rapid anode corrosion. Recently, the types of electrolyte are under review (Mokhtar et al., 2015). Electrolytes that are used for Al-air batteries are; aqueous electrolytes, acidic solutions, neutral salt solutions, alkaline solutions, non-aqueous, aprotic electrolytes and solid-state electrolytes. However, metal-air batteries have a specific requirement for the electrolyte. In the case of aqueous electrolytes, most usually use an alkaline electrolyte because the ORR is more favorable in an alkaline electrolyte. Further, aqueous electrolytes are inexpensive, easily available and have high ionic conductivity. As for the alkaline electrolyte, it provides faster kinetic reaction but has lower potential compared with acidic electrolytes. The two common solutions used in aluminum electrolyte are, namely NaOH and KOH. The alkaline solution exhibits better aluminum-air performance but it also shortens the discharge voltage due to high corrosion.

Table 2.2 shows the types of electrolytes that have been employed for Al-air batteries; advantages and disadvantages are seen below.

Type of electrolyte	Advantage	Disadvantage	Reference
Liquid electrolyte	<ul style="list-style-type: none"> - Faster reaction kinetics - Lower overpotential - Low cost - High ionic conductivity 	<ul style="list-style-type: none"> - High corrosion and self-corrosion - Easy evaporated - Specific electrochemical window - Low specific capacity 	(Mokhtar et al., 2015)
Solid	<ul style="list-style-type: none"> - Reduced hydrogen evolution - Reduced flooding of electrolyte - Flexible for ionic transport with 	<ul style="list-style-type: none"> - Specific electrochemical window - Low specific capacity - Passivation 	

	amorphous structure		
Ionic liquid	<ul style="list-style-type: none"> - Reduced corrosion - Thermal stability - Low toxicity - High boiling point - Low vapor pressure - High oxidation potential 	<ul style="list-style-type: none"> - Expensive - Low ion diffusion -High viscosity 	
Organic	<ul style="list-style-type: none"> - High oxidation potential - Low viscosity - Reduced corrosion - Reduced hydrogen gas evolution 	<ul style="list-style-type: none"> - Electrolytes decomposes in some type of organic solution 	

2.1.4 Ion exchange membranes

Ion exchange membranes divide the cell into two hydraulically separated compartments. They function as barriers to convection and diffusion, while permitting selective migration of ions. These materials have chemically designed pores of molecular size, typically in the range of 10^{-9} – 10^{-8} m. Ion exchange membranes include fluorocarbon and hydrocarbon materials that have ion exchange groups distributed throughout their structure. Normally, the membrane is a thin sheet of polymer that is designed to allow passage of either anions or cations, but not both (Santos. & Sequeira., 2013). An ion-permeable separator is used to separate the cathode from the anode. Ion exchange semi-permeable membranes are composed of ionic head groups attached to polymer matrices. They consist of two types: cation and anion. In the case of the Al-air battery, anion membrane was used. Alkaline anion exchange membranes form the following anions i.e. OH^- , HCO_3^- and CO_3^{2-} (Hagesteijn, Jiang, & Ladewig, 2018).

2.1.5 Battery performance evaluation and effect of parameters.

Generally, the performance of an electrochemical cell is evaluated by open circuit voltage (OCV), power density and polarization curves. In some cases, the efficiency of the battery

can also be calculated. For the aluminum-air battery, current efficiency can be evaluated in order to indicate the utilization of electrical energy supplied to regenerate aluminum.

2.1.5.1 Open Circuit Voltage (OCV)

OCV is the potential difference measured at zero current state. It represents equilibrium cell potential which includes some activation and resistance loss, as demonstrated by Eq. 2.1:

$$E_{cell} = E_{cathode} - E_{anode} \quad (\text{Eq. 2.1})$$

where E is electrode potential and superscript 0 stands for standard state.

Theoretically, the OCV of an Al-air battery is about 2.70 V. However, the actual OCV and theoretical OCV is different in this case. The theoretical OCV is the equilibrium cell voltage but the actual OCV includes some losses to activation and resistance. The measured OCV of an Al-air battery is about (1.4 – 1.6) V.

2.1.5.2 Polarization curve and overpotential

A polarization curve explains the relationship of the cell voltage and applied current. When an external electrically load changes, cell voltage changes according to the current. Fig 2.2 depicts the polarization with overpotentials of the Al-air battery. The curve can be divided into three regions based on the dominant overpotential: activation, ohmic and concentration.

A) Activation overpotential

The activation overpotential is the energy loss from the activation of the electrochemical reaction. This loss dominates the early region to the middle region of the polarization curve ranging from OCV to the initial constant slope zone. As for the Al-air battery, activation overpotentials are caused by the reactions (2.1) and (2.2). As regards aluminum activation loss, concentration of the electrolyte and surface area of the aluminum are major parameters that affect this loss. The major activation overpotential is the activation loss of air electrode. There are various parameters that affect the air overpotential due to the complexity and sluggishness of the oxygen reduction and evolution reaction. The parameters that are involved in the mass transfer of oxygen mainly concern the diffusivity of oxygen in the gas diffusion layer.

B) Ohmic overpotential

Ohmic overpotential is the energy loss from the resistance of the electrode, electrolyte and other cell components. This loss dominates the middle region of the curve ranging over the constant slope zone. The parameters that affect the resistance in the cell contributed to Ohmic loss. For instance, the changing concentration of KOH solution affects the conductivity of the electrolyte.

C) Concentration overpotential

Concentration overpotential is the energy loss from the depletion of the reactant due to mass transfer limitation. This loss dominates the high current region of the curve as demonstrated by the rapid drop in the discharging cell voltage or the high surge in the charging voltage. As for the Al-air discharging battery, diffusion limit of oxygen to the air cathode is the predominant contribution to the concentration loss; mass transfer limit of hydroxide ion is the second dominant contribution. Most of the Al-air batteries suffer from oxygen diffusion limit before the hydroxide ion transfer limit even occurs.

2.1.5.3 Power density

Normalized specific power is called power density. Generally, cell power does not guarantee whether cell performance is high or low. Power needs to be normalized to the active area of the electrode. In the case of the Al-air battery, the active area is usually the air cathode area as demonstrated:

$$P_{density} = \frac{net\ power}{active\ area} = I_{density} \times E_{cell} \quad (\text{Eq. 2.2})$$

2.1.5.4 Specific capacity (S.C.)

In the case of Al-air battery, cell performance is evaluated by its energy consumption. In this study, specific capacity (Q_{net}) is defined as the ratio of the aluminum electric charge to the net weight of aluminum that is applied:

$$Q_{net} = \frac{electric\ charge\ (mAh)}{net\ weight\ of\ aluminum\ (g)} \quad (\text{Eq. 2.3})$$

Cell performance can be calculated according to utilization percentage, namely: by the ratio of net specific capacity and the theoretical specific capacity of aluminum. Theoretical capacity is estimated by Faraday's law:

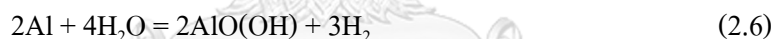
$$Q_{theoretical} = \frac{nF}{M_w} \times \frac{1000}{3600} \frac{mAh}{g} \quad (\text{Eq. 2.4})$$

where n is 3 of aluminum produced electron, F is 96485 sA/mole and M_w of pure aluminum is 27 g/mole as demonstrated:

$$\%utilization = \frac{net\ capacity}{theoretical\ capacity} \times 100 \quad (\text{Eq. 2.5})$$

2.1.6 Corrosion and mechanism of aluminum in electrolyte.

Both the reaction and product of aluminum depend on temperature. Thus, the possible reactions of aluminum with water are as follows (Digne, Sautet, Raybaud, Toulhoat, & Artacho, 2002):



These reactions depend on the temperature according to their level of hydration. Possible reactions of aluminum with water can produce the following: $Al(OH)_3$, $AlO(OH)$ and Al_2O_3 . All of these reactions produce the same amount of hydrogen with respect to the amount of aluminum. However, they differ in the amount of water that is required for these reactions. These reactions are highly exothermic. When room temperature reaches 280°C , it enables $Al(OH)_3$ to be produced and is most stable product. When the temperature is increased from 280 to 480°C , $AlO(OH)$ is produced; this also is most stable. In addition, the temperature above 480°C produces Al_2O_3 which is again a most stable product.

Aluminum is always sensitive in an alkaline based electrolyte. Normally, the corrosion mechanism of pure aluminum in alkaline solution is brought about through hydroxide film

formation. The hydroxide film is formed due to the migration of hydroxide ions through the oxide layer on the aluminum surface. The reaction steps are shown in (2.8) - (2.14):

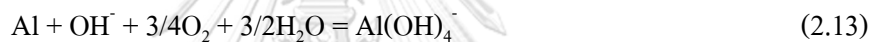
Anode reaction:



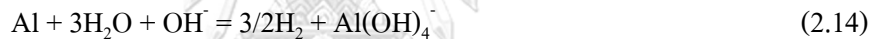
Cathode reaction:



Total reaction:



and



However, the mechanism depends on the type of electrolyte used. In this case, aluminum is in contact directly with the methanol based electrolyte, combined with 3M KOH mixed solution. Corrosion potential (E_{corr}) is discussed in Chapter 4 as Tafel polarization. In addition, the prediction of aluminum mechanism can be modified by EIS technique. The basic principle of aluminum mechanism is illustrated as follows:

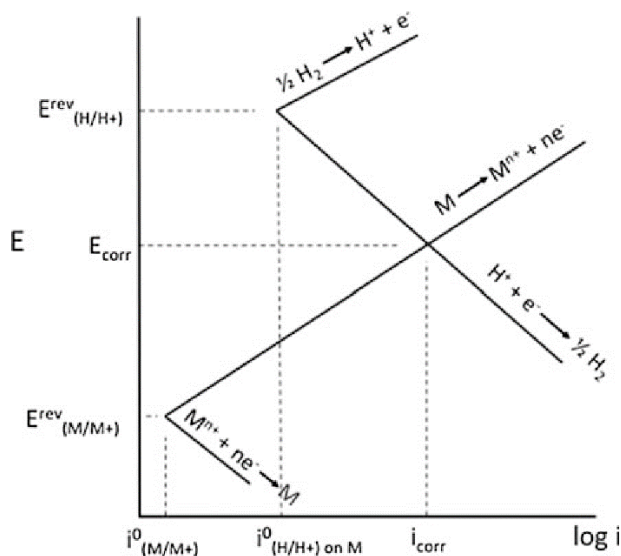


Figure 2.4 schematic Evans diagram for the corrosion of metal 'x' by an acid showing the application of mixed potential theory (Frankel, 2016)

Corrosion potential is called open circuit potential (OCV). Corrosion potential indicates that the value depends on the rate between anodic and cathodic reactions. Fig. 2.4 shows that the schematic Evans diagram can imagine the relationship of anodic and cathodic reactions indicating that they intercept together at one point. In this case, $E^{rev}_{(H/H^+)}$ is hydrogen evolution reaction and $E^{rev}_{(M/M^+)}$ is aluminum dissolution reaction. The potential as these lines intersect is the corrosion potential (E_{corr}). Furthermore, i_{corr} represents the corrosion current density where $i_{0, M/M^+}$ and $i_{0, H_2/H^+}$ are exchange current densities for aluminum dissolution and hydrogen evolution on aluminum.

2.1.6.1 Tafel polarization

The potentiodynamic was used to determine the polarization curve. In this work, a three-electrode cell was used consisting of: a counter electrode, a working electrode and a reference electrode. Fig. 2.5 shows an example of Tafel polarization curve:

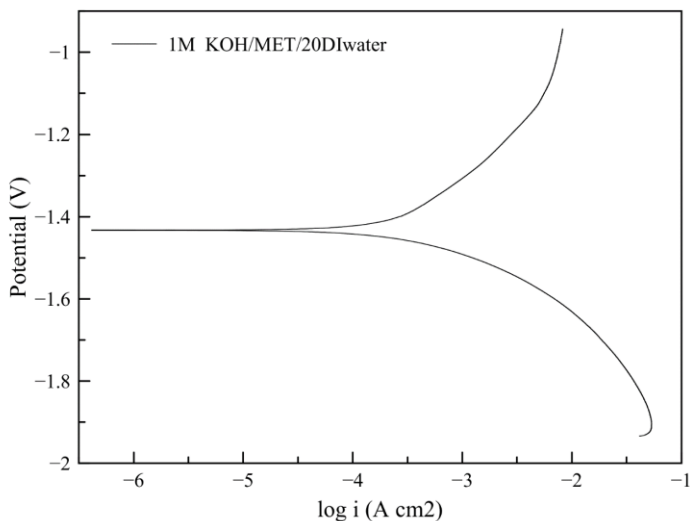


Figure 2.5 the example of Tafel polarization of aluminum in methanol based electrolyte

Polarization resistance was calculated by Butler-Volmer and Stern-Geary equations. The electrochemical polarization parameters consist of; corrosion potential (E_{cor}), corrosion current density (I_{corr}), anodic slope (β_a), cathodic slope (β_c) and polarization resistance (R_p). The extrapolation of the linear Tafel curve determines the electrochemical polarization parameters. The Tafel equations employ the Butler-Volmer equation that is described as follows (Frankel, 2016):

$$I = I_{corr} \left(e^{\frac{2.303(E-E_{corr})}{\beta_a}} - e^{-\frac{2.303(E-E_{corr})}{\beta_c}} \right) \quad (\text{Eq. 2.6})$$

where I is the measured current, I_{corr} is the corrosion current, E is the electrode potential, E_{corr} is the corrosion potential, β_a and β_c are the Tafel slopes of anodic and cathodic partial reactions. Since the potentials are close to E_{corr} , the Tafel curves can be approximated as a straight line. The slope of this line is called the polarization resistance (R_p), which can be determined using the Stern-Geary equation (Abdel-Gawad, Osman, & Fekry, 2018):

$$R_p = \frac{\beta_a |\beta_c|}{2.303 I_{corr} (\beta_a + |\beta_c|)} \quad (\text{Eq. 2.7})$$

The unit of resistance (R_p) is the transition resistance between the electrodes and the electrolyte.

Chapter 3

Literature review

3.1 Literature review of the behavior of aluminum's corrosion

A major complication, when applying aluminum in alkaline based batteries, is its high corrosion rate in an electrolyte. Aluminum corrosion has been happening over many years. Moghadam, Shabani-Nooshabadi, & Behpour (2017) proposed using urea and thiourea, an aluminum alloy, in strong alkaline electrolyte. The work was studied in half-cell 5M KOH solution along with an additive. The half-cell was investigated via hydrogen evolution, Tafel polarization as well as EIS techniques. Battery performance was investigated by galvanostatic discharge. The maximum capacity density was found to be 1282 mAh/g and provided 600 s at a discharge current 20 mA/cm^2 in 25 mM thiourea.

D. Wang et al (2015) studied aluminum alloy (AA5052) in an alkaline electrolyte with an organic rare-earth complex additive for aluminum-air batteries. The work was carried out in half-cell 4M KOH solution with an amino-acid and rare earth additive (Cerium nitrate hexahydrate). EIS was employed to the model to explain the behavior of AA5052 in the electrolyte. The EIS showed that the polarization resistance of 40 mM of L-cysteine combined with Cerium nitrate hexahydrate had higher resistance. Thus, it was effective in preventing AA5052 alloy from self-corrosion effectively.

Deepa & Padmalatha (2017) demonstrated the corrosion behavior of 6063 aluminum alloy in phosphoric acid and in sodium hydroxide electrolyte at different temperatures and different concentration. Results showed that the corrosion occurred in alkaline media rather than acidic electrolyte. When the temperature increased, the corrosion rate increased.

J.-B. Wang, Wang, Shao, Zhang, & Cao (2007) discussed the corrosion and electrochemical behavior of pure aluminum in alkaline methanol solutions; concentration of KOH and water content varied. Consequently, it was found that corrosion rate increased when water content in KOH methanol increased. However, corrosion rate stayed still low when the content of water was less than 20%.

J. B. Wang et al (2009) reported the corrosion of aluminum (pure 99.9995%) in additives which contained an alkaline methanol-water mix solution: Zinc oxide and hydroxytryptamine. When additives were added, the cathodic polarization found that the OCV came to positive shift. The galvanostatic discharge at 20 mA/cm^2 had a long life around 85,000 s.

Mukherjee & Basumallick (1996) studied the behavior of aluminum dissolution in an alkaline aqueous 2-propanol solution. 1M KOH was used in the work. Corrosion almost vanished at 56 vol% of 2-propanol. This suggested that the use of the small concentration of 2-propanol in alkaline for aluminum-air batteries may be useful for increasing anode efficiency.

Chaubey, Yadav, Singh, & Quraishi (2017) reported on a study of leaf extracts for corrosion inhibition of aluminum alloy in alkaline electrolyte. Results found that temperature was significant for such corrosion. EIS was employed to calculate inhibition efficiency.

Danny Gelman, Lasman, Elfimchev, Starosvetsky, & Ein-Eli (2015) examined the aluminum corrosion in alkaline electrolytes using a hybrid organic inhibitor based on poly (ethylene glycol) di-acid (PEG di-acid) and Zinc oxide (ZnO). An Al-air battery was also studied in the work. Optimal inhibition effect was obtained in a solution containing hybrid inhibitor containing 500 ppm of PEG di-acid and 16 g/l ZnO. This system provided maximum discharge capacity of 70 mAh/cm^2 at a discharge current of 25 mAh/cm^2 .

Mutlu & Yazıcı (2018) proposed copper-deposited aluminum for an Al-air battery. NaOH was used for the electrolyte. The copper lead to an increase in efficiency when the alkaline electrolyte decreased due to aluminum corrosion. Maximum utilization was 83.1% of Alloy/Cu-Ed and the average discharging of 0.0447 A at 1 V via galvanostatic discharge technique.

3.2 Literature of an aluminum-air battery

Cho, Park, Lee, & Kim (2015) studied the different grades of aluminum using commercial grade (pure 99.5%) and pure aluminum 99.99%. The impurity of the two types of aluminum used were examined to compare the Al-air performance. The percentage utilization of pure aluminum was 71.96% while commercial grade was 76% at 0.8V discharge voltage. Results found that both discharge performances were similar. Thus, it was found that the commercial grade could be used as a promising anode because it was cheaper than pure aluminum.

Fan, Lu, Leng, Sun, & Chen (2015) studied the effect of crystal orientation on the aluminum anode of the aluminum-air batteries in alkaline electrolytes. The specific type of aluminum was examined. Thus, it was observed that the single crystal of aluminum provided the highest density capacity greater than polycrystalline.

X. Han et al (2018) presented a microbial electrolysis cell powered by an aluminum-air battery for hydrogen generation. The Al-air battery supplied the energy as well as produced hydrogen gas when used in strong alkaline.

D. Gelman, Shvartsev, & Ein-Eli (2014) demonstrated an Al-air battery based on an ionic liquid electrolyte. The electrolyte used in this work was 1-ethyl-3-methylimidazolium oligo-fluoro-hydrogenate $\text{EMIm}(\text{HF})_{2,3}\text{F}$. The performance of the $\text{Al} \mid \text{EMIm}(\text{HF})_{2,3}\text{F} \mid \text{air}$ battery provided a current density up to 1.5 mA/cm^2 , capacity above 140 mAh/cm^2 and utilization around 70%.

Tang, Lu, Roesky, Wang, & Huang (2004) examined the effect of zinc on the aluminum anode of an Al-air battery. The electrolyte used was aqueous 4M NaOH as well as NaCl solution; ZnCl_2 was an additive. When NaOH was used to investigate the Al alloy (Al-In-Zn), it was found that zinc can lower anodic polarization. The surface of aluminum was covered by $\text{Zn}(\text{OH})_2$. Consequently, the hydrogen evolution decreased.

Di Palma, Migliardini, Caputo, & Corbo (2017) proposed hydrogel as electrolytes for Al-air batteries. Xanthan and k-carragenan were used to make the (1 and 8)M KOH hydrogel electrolyte. The work was checked for ionic conductivity. The capacity was examined via galvanic three-electrode cell. The maximum capacity discharge was found to be 53 mAh/cm^2 and energy power reached up to 33 mWh/cm^2 .

Shvartsev, Gelman, Amram, & Ein-Eli (2015) investigated the use of an ionic liquid based electrolyte for an Al-air battery. The work employed $\text{EMIm}(\text{HF})_{2,3}\text{F}$, EMImOTF and EMImTFSI . Results found that $\text{EMIm}(\text{HF})_{2,3}\text{F}$ can provide a lifetime of 45 hours. The capacity provided up to 160 mAh/cm^2 .

Mori (2017) researched the electrochemical properties of a rechargeable Al-air battery. The work was interesting since it use an aluminum terephthalate as a metal-organic framework and 1-ethyl-3-methylimidazolium chloride as an ionic electrolyte. The capacity of 1 cycle was

around 154 mAh/g and 25 cycle was around 28 mAh/g. This confirmed that the electrolyte did not observe the passivation on the aluminum surface.

Mori (2015) studied the capacity recovery of an Al-air battery by refilling salty water in the electrolyte. The refilling of salty water placed a layer of activated carbon between NaCl and the electrodes. Maximum capacity was around 400 mAh/g after refilling at 20 cycles. The maximum lifetime of the battery was around 60 hrs. at 1 mA/cm².

Kruehong studied the performance of an Al-air battery in mixed solutions between NaOH and NaCl. The research found that the mixing of NaCl and NaOH reduced self-corrosion and increased the energy density of the Al-air battery. The maximum specific capacity and energy density provided 137.28 mAh/g and 145.66 Wh/kg. The maximum life time of discharge was 10 hrs.

Takashi Hibino, Kobayashi, & Nagao (2013) demonstrated an Al-air battery using solid state with hydroxide ion-conducting Sb(v)-doped SnP2O7 electrolyte. The work provided OCV of 1.6V and a discharge capacity of 800 mAh/g.

Zhang et al (2014) observed the solid state of an alkaline electrolyte for an Al-air battery. The work used polyacrylic acid (PAA) for an alkaline based gel electrolyte. The capacity and energy density provided 1166 mAh/g and 1230 mWh/g respectively. The lifetime of the battery was around 7 hrs.

Mori (2014) studied the secondary battery of an Al-air battery. The work used an aluminum ion conductor Al₂(WO₄)₃ for supporting a solid state of aluminum that was a byproduct of Al. The work illuminated their innovation and the possibility of a rechargeable Al-air battery. Salt water (NaCl) was used for the electrolyte. The maximum capacity was of 5.472 mAh/cm² at 0.2 mA/cm².

Fan & Lu (2015) examined different grain sizes for an Al-air battery. The ideal metal of aluminum was used in the work. 4M NaOH was used for the electrolyte. The maximum capacity density was 2885 mAh/g and utilization reached 96.8% at 50 mA/cm². The battery system produced maximum hydrogen evolution rate which was 0.418 ml/cm²min.

B. Han & Liang (2006) reported on a neutral electrolyte (3.5% NaCl solution) for an Al-air battery. The aluminum alloy used in this research consisted of: Ga, In, Sn, Bi, Pb and Mn. The

voltage of this system stayed at 1.1 V discharging at 290 mA for 140 hrs. The utilization of aluminum was around 44%.

Ma, Wen, Gao, & Li (2014) examined an aluminum alloy made of Al-Mg-Ga-Sn, Al-Mg-Ga-Sn-Mn and Zn. The neutral 2M NaCl was used as an electrolyte. The maximum operating voltage was 1.23 V for 85.3% of anodic efficiency.

Fan, Lu, & Leng (2015) focused on the structure of aluminum in neutral (2M NaCl) and alkaline (4M NaOH, 4M KOH) electrolytes for aluminum. The ultrafine-grained and coarse-grained aluminum were studied. The neutral salt provided the highest polarization resistance. The performance of the Al-air battery improved using NaOH and provided the capacity of 1648 mAh/g and 2308 mAh/g for the ultrafine-grained and coarse-grained aluminum, respectively. However, the KOH electrolyte performed better than the NaOH electrolyte. Maximum capacity was 2479 mAh/g and energy density was 3594 Wh/kg discharging at 10 mA/cm².

Zhuk, Kleimenov, Udal'tsov, Kiseleva, & Tarasenko (2018) proposed a cylindrical cell design for an Al-air battery. The new design was fabricated for comparison with a flat aluminum-air battery. The result was that the mass loss of cylindrical design was lower than the flat design having the same discharging. The power energy provided around 350 Wh/kg.

Levy, Auinat, & Ein-Eli (2018) examined organic non-aqueous electrolytes and tetrabutylammonium fluoride tri-hydrate (TBAF-3H₂O) was used. The best additive proved to be propylene carbonate (PC). Maximum capacity reached 30 mAh/cm² at 2.5M concentration of TBAF-tri-hydrate salt.

Hopkins, Shao-Horn, & Hart (2018) noted that oil-displacement suppressed aluminum's corrosion in an Al-air battery. An underwater-oleophobic was used to clear the passivation of the aluminum surface. The oil-displacement was clear time by time by pumping. The cathode was a Nano-manganese catalyst with carbon coated on nickel mesh. The electrolyte was 4M NaOH. Maximum specific capacity was 2697 mAh/g discharging at 250 mA/cm².

3.3 Literature of dual-electrolytes, flow system and other types of battery

Recently, in the research, it was reported that a dual-electrolyte was modified from a battery based fuel cell. Chen, Xuan, Wang, & Leung (2017) developed the capacity with microfluidic Al-air cell using dual-electrolytes system. The cell consisted of two electrolytes: an

anolyte and a catholyte. The catalyst was activated with Pt/C. The system employed was non-direct counter-flow. Both electrolytes used membraneless to separate their electrolytes. Results showed that the OCV underwent a negative shift when the electrolyte's concentration increased. At 3M KOH, the highest short circuit current density was found to be 8.63 mA/cm^2 . When the water content was 60%, the highest short circuit current density was 55.2 mA/cm^2 . However, it was seen that 0%water provided the highest capacity density of the system, namely 2507 mAh/g .

Chen, Leung, Xuan, & Wang (2017) studied a mixed-pH dual-electrolyte from microfluidic technology to develop an aluminum-air cell. The mixed-pH dual-electrolyte design was for increasing thermodynamic potential using different alkaline and acid with membraneless. The flow rate and thickness of the electrolyte were examined. The Al-air cell was Y-shaped in design. The electrolytes used aqueous KOH and H_2SO_4 solution. The catalyst was activated with Pt/C. The research examined the difference between single and dual-electrolyte.

L. Wang et al (2014) researched a high-capacity dual-electrolyte aluminum-air electrochemical-cell. Methanol was used for the anolyte while aqueous alkaline was used for the catholyte. The cell had two chambers for containing both electrolytes. Pt/C was used for supporting the cathode. Results found that the short circuit current density in the single electrolyte was higher than the dual-electrolyte. However, the discharge capacity of the dual-electrolyte took a longer time than the single electrolyte. Maximum discharge was around 2500 mAh/g at 10 mA/cm^2 and voltage around -0.8 V .

L. Li & Manthiram (2013) focused on: the use of dual-electrolyte lithium-air batteries, the influence of catalysts, temperature and solid-electrolyte conductivity, as regards efficiency and power density. The work included the study of half-cell test and full-cell test. The maximum power density was 40 mW/cm^2 . The battery conversion reached 80% at 2 mA/cm^2 in temperature of 40 degree Celsius.

L. Li, Zhao, & Manthiram (2012) studied a non-aqueous electrolyte for an anolyte and aqueous electrolyte for a catholyte. The work developed a dual-electrolyte rechargeable Li-air battery with a phosphate buffer cathode. LTAP was used for separating both electrolytes. The system provided a discharge capacity of 221 mAh/g . Energy density was 770 Wh/kg and current density was 0.5 mA/cm^2 which was rechargeable after 20 cycles.

Table 3.1. Literature review of the corrosion behavior of aluminum

Description	Remarkable conclusion	Reference
The Al alloy with alkaline electrolyte used urea and thiourea for inhibiting the corrosion	The maximum capacity density was 1282 mAh/g of 600 s; discharge current was 20 mA/cm ² at 25 mM thiourea.	(Moghadam et al., 2017)
The Al alloy used the Cerium nitrate hexahydrate for additive	The resistance of 40 mM L-cysteine/Cerium nitrate hexahydrate was higher; it prevented Al alloy from self-corrosion.	(D. Wang et al., 2015)
Aluminum alloy in phosphoric acid and in sodium hydroxide electrolyte	The corrosion occurred in alkaline electrolyte rather than in acidic electrolyte. The corrosion rate increased when temperature increased.	(Deepa & Padmalatha, 2017)
Pure Al in alkaline methanol solutions	The corrosion rate increased when water content in KOH methanol increased, but it stayed low when the content of water was less than 20%.	(J.-B. Wang et al., 2007)
Al in alkaline methanol-water mix solution with additives of Zinc oxide and hydroxytryptamine	The OCV reached positive shift when additive was added. The galvanostatic discharge at 20 mA/cm ² had a long life around 85,000 s.	(J. B. Wang et al., 2009)
Al in alkaline aqueous 2-propanol solution.	The corrosion was almost suppressed at 56 vol% of 2-propanol.	(Mukherjee & Basumallick, 1996)
Leaf extracts for corrosion inhibition on Al alloy in alkaline electrolyte	The temperature was significant as regards corrosion inhibition efficiency.	(Chaubey et al., 2017)
Al in electrolyte used the	500 ppm of PEG di-acid and 16 g/l ZnO	(Danny Gelman

hybrid organic inhibitor based on poly (ethylene glycol) di-acid (PEG di-acid) and Zinc oxide (ZnO).	was optimization for this system. The maximum discharge capacity was 70 mAh/cm ² at discharge current of 25 mAh/cm ² .	et al., 2015)
Copper-deposited aluminum for aluminum-air battery	The maximum utilization was 83.1% of Alloy/Cu-Ed; average discharging was 0.0447 A at 1 V by galvanostatic discharge.	(Mutlu & Yazıcı, 2018)

Table 3.2. Literature review of aluminum-air battery

Description	Performance/remarkable conclusion	Reference
Al-air battery with different grades of aluminum (pure Al 99.99% and Al 99.5%)	Pure Al lost weight more than Al 99.5%, Maximum capacity during discharge was 1635.62 As or 454.34 mAh.	(Cho et al., 2015)
Comparison between single crystals Al and polycrystalline Al.	Polycrystalline Al produced H ₂ much more single crystal Al; the maximum capacity density was 2541.4 mAh/g with (001) single crystal at 10 mA/cm ² for 3 hrs.	(Fan, Lu, Leng, et al., 2015)
Al-air battery produced H ₂ for supporting the microbial electrolysis cell	The Al-air battery was useful in the production of H ₂ for supporting other systems without external circuit.	(X. Han et al., 2018)
Al-air battery used the EMIm(HF) _{2,3} F of Ionic liquid for electrolyte	Capacity above 140 mAh/cm ² with utilization around 70% at 1.5 mA/cm ² .	(D. Gelman et al., 2014)
Effect of Zn on Al electrode for an Al-air battery	Zn can reduce self-corrosion of Al surface.	(Tang et al., 2004)
Xanthan and k-carragenan based alkaline hydrogel as electrolytes of Al-air battery	The maximum capacity discharge was 53 mAh/cm ² . The energy power reached 33 mWh/cm ² .	(Di Palma et al., 2017)
EMIm(HF) _{2,3} F, EMImOTF and EMImTFSI as ionic	The capacity provided up to 160 mAh/cm ² . The utilization was around 70%.	(Shvartsev et al., 2015)

liquid for the Al-air battery		
Rechargeable of the Al-air battery using metal-organic framework	The capacity of 1 cycle was around 154 mAh/g and 25 cycle was around 28 mAh/g. Al(OH) ₃ and Al ₂ O ₃ did not occur.	(Mori, 2017)
Refilling salty water electrolyte for Al-air battery	The maximum capacity was around 400 mAh/g after refilling at 20 cycles. The maximum of battery's lifetime was around 60 hours at 1 mA/cm ² .	(Mori, 2015)
The Al-air battery in mixed solutions between NaOH and NaCl.	The maximum specific capacity and energy density were 137.28 mAh/g and 145.66 Wh/kg. The maximum lifetime of discharging was 10 hrs.	(Kruehong)
The Al-air battery using solid state for electrolyte	The work provided OCV of 1.6V and discharge capacity of 800 mAh/g using Pt/c cathode electrode.	(Takashi Hibino et al., 2013)
Different grain sizes for the Al-air battery	The maximum capacity was 2885 mAh/g; utilization 96.8% at 50 mA/cm ² , hydrogen evolution rate was 0.418 ml/cm ² min.	(Fan & Lu, 2015)
Neutral electrolyte (3.5% NaCl solution) in Al alloy for Al-air battery	The battery stayed at 1.1 V discharging at 290 mA for 140 hrs. The utilization of aluminum was around 44%.	(B. Han & Liang, 2006)
Al in neutral (2M NaCl) and alkaline (4M NaOH, KOH)	The maximum capacity was 2479 mAh/g. Energy density was 3594 Wh/kg discharging at 10 mA/cm ² at KOH electrolyte.	(Fan, Lu, & Leng, 2015)
The cylindrical cell design for Al-air battery.	The possibility of power energy provided around 350 Wh/kg.	(Zhuk et al., 2018)
The non-aqueous electrolytes (TBAF-3H ₂ O) for Al-air	The maximum capacity was 30 mAh/cm ² of the TBAF-3H ₂ O based electrolyte with	(Levy et al., 2018)

battery	additive of propylene carbonate.	
The oil-displacement suppressed the aluminum's corrosion for Al-air battery.	The maximum specific capacity was a 2697 mAh/g with discharging of 250 mA/cm ² .	(Hopkins et al., 2018)

Table.3.3 Literature review of dual-electrolyte system

Description	Performance/remarkable conclusion	Reference
The microfluidic Al-air cell used dual electrolytes (DI-water and methanol) system with membraneless.	The maximum current density was of 8.63 mA/cm ² at 3M KOH and 55.2 mA/cm ² with content 60% of water. The capacity density of pure methanol provided of 2507 mAh/g with Pt/c of cathode.	(Chen, Xuan, et al., 2017)
Mixed-pH dual-electrolyte from microfluidic to develop an Al-air cell.	The flow rate was influenced to the current density and power density.	(Chen, Leung, et al., 2017)
The dual-electrolyte aluminum-air electrochemical-cell.	The maximum discharge was around 2500 mAh/g at 10 mA/cm ² and voltage around 0.8 V with Pt/c of cathode.	(L. Wang et al., 2014)
The non-aqueous as an anolyte and aqueous as a catholyte for Li-air battery	The capacity was 221 mAh/g, energy density provided of 770 Wh/kg and current density of 0.5 mA/cm ² for rechargeable at 20 cycle.	(L. Li & Manthiram, 2013)

Chapter 4

Methodology

4.1 Material and chemicals

An aluminum (Al) plate with a purity of 99.99% was used as the working electrode in the half-cell test and the battery's anode current collector. Nickel foam (99.97%) purity, 1 mm thick, was supplied by Qijing Trading Co., Ltd., and was used as the cathode current collector. The electrolyte of the half-cell test contained methanol of AR grade and potassium hydroxide pellets (KOH) AR grade, as purchased from Quality Reagent Chemical Product (QReC). The cathode electrode used carbon black (Vulcan®BP2000, Cabot Corporation), Polytetrafluoroethylene (PTFE powder, 1 μm , Sigma-Aldrich), Toluene AR 99.5% (LOBA CHEMIE PVT. LTD), Ethanol 99.9% (QReC), Poly (styrene-co-butadiene) and manganese (IV) oxide (MnO_2 , 5 μm 99.99%, Sigma-Aldrich). CARBOPOL940 polymer (CBP940) was used as the cathode's electrolyte. All chemicals were used as accepted without any further purification. Both electrolytes, in the full-cell test, were separated by the anion-exchange membrane (Membrane International Inc., USA). A peristaltic pump controlled the flow rate of the electrolyte.

4.2 Hydrogen evolution test

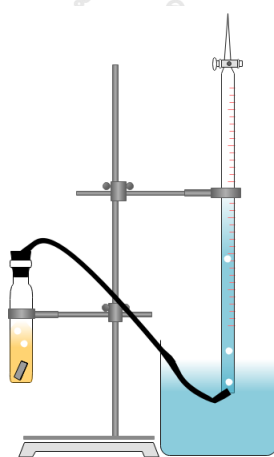


Figure 4.1 hydrogen evolution collection

Aluminum samples ($10 \times 10 \times 0.19$) mm. were placed in a drainage device which consisted of a 50 ml tube and a gas guide tube (ID of 0.5 mm). The 50 ml tube contained 3M KOH solution along with 40 ml of deionized water. The burette allowed the volume of evolved hydrogen gas to be measured as a function of time. Before testing the aluminum, samples were cleaned using methanol five times. Reaction rates were determined by the slope of the straight lines in the gasometry plots.

4.3 Half-cell test

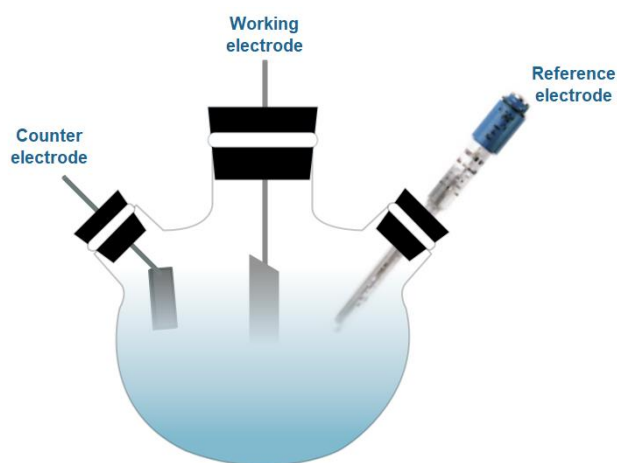


Figure 4.2 Three-electrode cell design

The half-cell test investigated the use of methanol by varying the amount of deionized water used i.e. (0, 5, 10 and 20)% of 3M KOH-methanol mixed solution. A three-electrode cell was used to study the electrochemical measurement and characterization. The three-electrode cell consisted of a platinum counter electrode (10×10) mm, Ag/AgCl reference electrode and an Al plate working electrode (10×10) mm. A potentiostat/galvanostat was employed to study electrochemical impedance spectroscopy (EIS) and Tafel polarization with unit software (AMETEK, PAR VersaSTAT3A). The aluminum working electrode was rinsed out by methanol three times before testing at room temperature. Then, EIS was examined at a frequency range of 100k Hz - 0.02 Hz. After that, Tafel polarization was performed at a scan rate of 5mV/s in the potential region cover at OCP minus 500 mV to positive 0 V vs. Ag/AgClreference. The experimental data were recorded in Zplots which were fitted using ZsimpWin software.

4.4 Full cell test

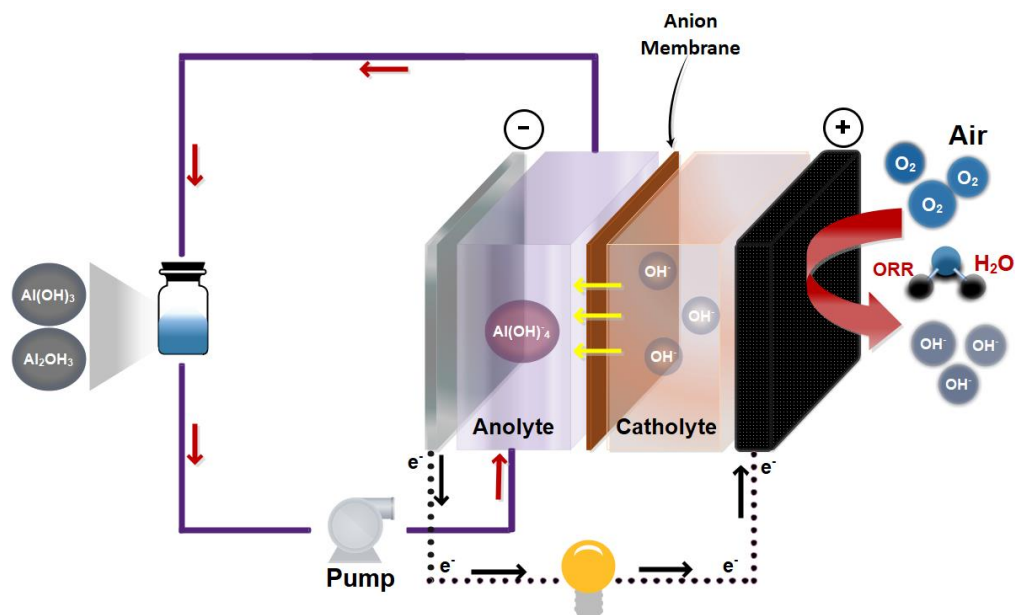


Figure 4.3 schematic illustration of an Al-air battery

Fig. 4.3 shows the schematic illustration of the Al-air cell structure of the dual-electrolyte system which was used for the battery. As illustrated, the anode consists of an anolyte and the cathode consists of a catholyte. Various amounts i.e. (0, 5, 10 and 20)% of deionized water with KOH in methanol solvent (KOH-CH₃OH) flowed through the anolyte via a peristaltic pump. The catholyte is a gel polymer electrolyte consisting of 3M KOH dissolved in deionized water. For each condition, a solution 1.2 wt% was obtained. Then, CBP940 was added to each condition. An anion-exchange membrane (30 × 30) mm. separated the two electrolytes. The anion-exchange membrane was activated with 5M NaCl aqueous solution for 24 hours. The operation was carried out at room temperature for all maintenance. The cathode electrode consisted of three-layers: a catalyst layer, a cathode current collector and a gas diffusion layer. The catalyst layer was attached to the catholyte. The catalyst layer was fabricated at 120 °C by casting together a mixture of MnO₂ and carbon black (2:3); the mixture was dissolved in toluene together with Poly(styrene-co-butadiene) which acted as the binder. The cathode current collector is nickel (Ni) foam. The gas diffusion layer was fabricated on nickel foam by casting at 350 C° and was

combined together with the composition of carbon black and PTFE (3:2) which was dissolved in ethanol. All conditions were repeated at least three times.

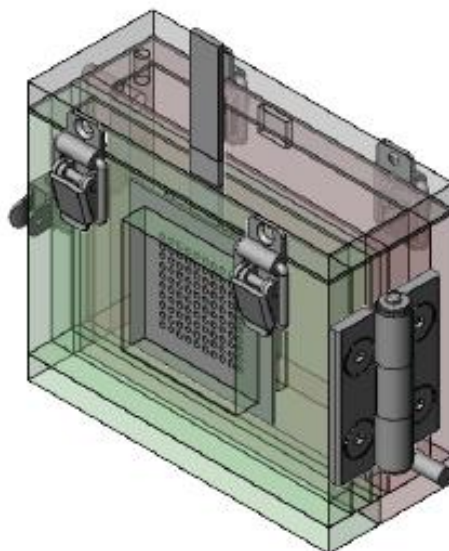


Figure 4.5 battery of cell experiment design

In Fig. 4.5 the battery used in the experiment is shown. The cell design consisted of: an aluminum (anode) | a chamber¹ for containing the anolyte | an anion exchange membrane (separator) | a chamber² for containing the catholyte | air (cathode). The active reaction of the cathode area was 4 cm^2 . The anode electrode was $(30 \times 40) \text{ mm}$ and 0.19 mm thick and weighed around 0.6 g . The anion exchange membrane was $(30 \times 30) \text{ mm}$. The distance between the cathode and anode electrodes was roughly 18 mm . Gel polymer was used for the catholyte to make sure that no liquid leaked out through a pore of nickel foam. The cell experiment design had a hole with a diameter of 0.5 mm for fixing the problem of a hydrogen gas leak. Battery performance was investigated by NEWARE (BTS7.6.0) software. The performance of the batteries depended on many factors: the type of cathode, thickness, flow rate and impurity of anode. Appendix A4, shows the aluminum-air battery design experiment.

Chapter 5

Results and discussion

In this research, pure aluminum (99.99%) in the organic electrolyte was modified for the Al-air battery which had a dual-electrolyte for the flow anolyte system. The behavior of aluminum's corrosion was investigated via Tafel polarization, electrochemical impedance spectroscopy (EIS) and hydrogen evolution.

5.1 The aluminum's corrosion in 3M KOH with anhydrous methanol, employing different percentage of deionized water, was investigated.

5.1.1 Hydrogen evolution

Typically, Al has self-corrosion which is a massive problem. In Fig. 5.1, it is noted that the linear variation for the volume of hydrogen gas is related according to the time for each condition. The volume of hydrogen can speculate how much aluminum consumed itself without discharging. The diagram indicates that hydrogen evolution is higher when deionized water's percentage is raised. Another effect of self-corrosion is the weight loss of aluminum after being immersed for 90 min. Results were weighed before and after testing. Fig. 5.2 shows the weight loss (ΔW) of aluminum in the electrolyte. The diagram indicates that the highest weight loss of aluminum occurred in the condition of 20% water; this condition contained the highest deionized water percentage.

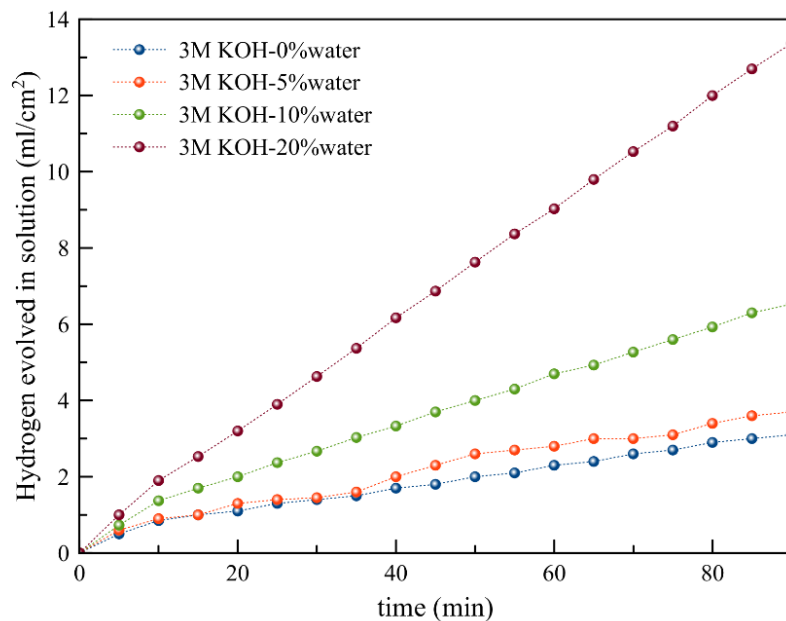


Figure 5.1 variation of the hydrogen volume evolved with time for aluminum in 3M KOH solution with different amount of deionized water (0, 5, 10 and 20)%wt.

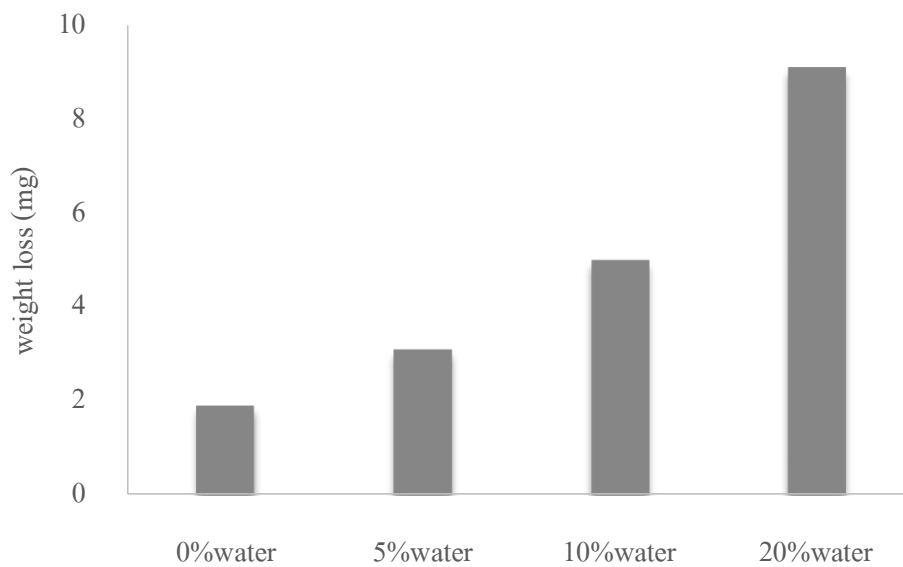
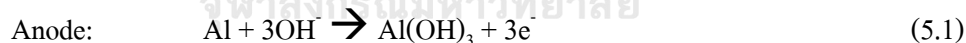


Fig 5.2 weight loss of aluminum versus immersion at 90 min. for aluminum in 3M KOH solution with different amount of deionized water (0, 5, 10 and 20)%wt.

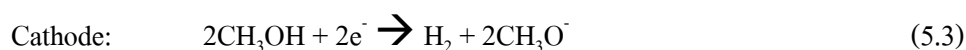
Table 5.1 Hydrogen gas evolution rate for aluminum in 3M KOH with anhydrous methanol, containing different amount of deionized water (0, 5, 10, 20)%wt.

Solution	ΔW (mg)	R_h (ml/cm ² min)
0%water	1.9	0.017
5%water	3.1	0.021
10%water	5	0.036
20%water	9.1	0.074

The hydrogen evolution rate of aluminum for each condition was calculated, as seen in Appendix A1. Table 5.1 records the hydrogen evolution rate (R_h) over the exposure period together with weight loss. The calculation of hydrogen gas evolution rate is explained by milliliter per centimeter as well as time. The condition of 0%water produced a hydrogen rate of 0.017 ml/cm² min. while the condition of 5%, 10% and 20% produced hydrogen rates of 0.021, 0.036 and 0.074 ml/cm² min., respectively. However, self-corrosion also occurred in the anhydrous methanol based electrolyte. This show is that aluminum is not durable in methanol based electrolyte and thereby produced hydrogen gas. Recent research suggests that aluminum reacts in methanol mixed with KOH solution; the corresponding electrode reactions are as follows (J. B. Wang et al., 2009):



Or



Or



Accordingly, the anhydrous methanol based electrolyte has two reactions. Both produced hydrogen gas though it was without deionized water. However, the aluminum in the anhydrous methanol based electrolyte consumed itself less than that which contained deionized water.

5.1.2 Tafel polarization

Tafel polarization was investigated via a three-electrode cell: namely an aluminum working electrode, Ag/AgCl reference electrode and a platinum counter electrode. The experiment was operated at room temperature. Fig. 5.3 shows the Tafel polarization of aluminum in 3M KOH solution with anhydrous and different amount of deionized water i.e. (0, 5, 10 and 20)%wt.

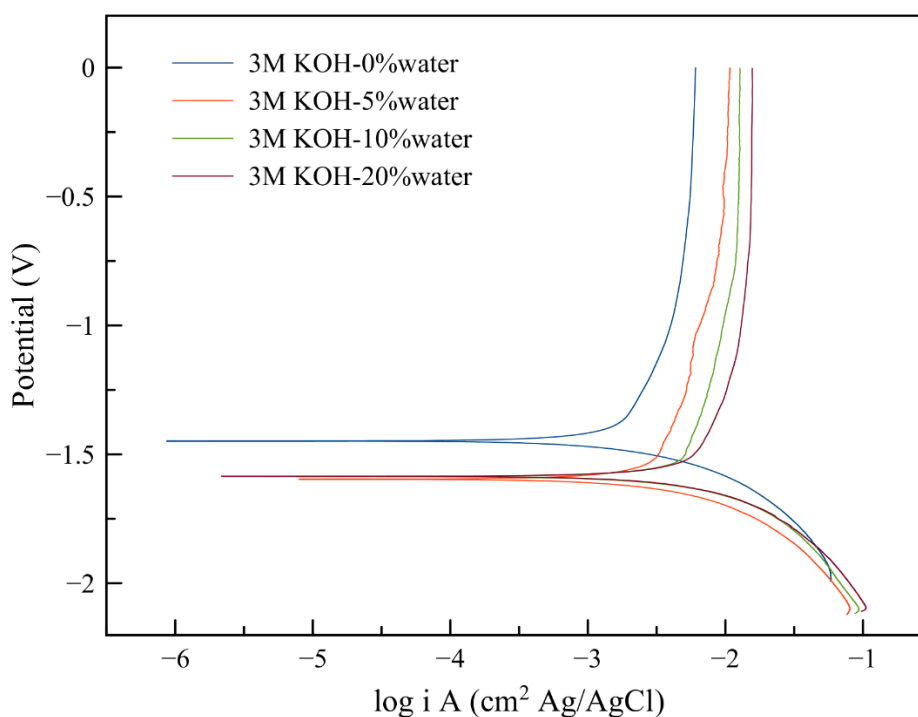


Figure 5.3 Tafel polarization curves of aluminum in 3M KOH methanol solution with various water contents; (blue) anhydrous methanol, (red) 5%wt of water, (green) 10%wt of water and (brown) 20%wt of water.

From Fig. 5.3, it can be seen that the OCV exposure in the anhydrous methanol based electrolyte was detected at -1.4477 V. The potential of OCV which contained deionized water reached a negative shift when the deionized water increased. The OCVs containing deionized water was around -1.59 V. Thus, the OCVs shifted to the negative at a potential that can possibly

estimate the range of hydrogen evolution. ΔE is the different OCVs between the samples reaction and standard potential half-cell of hydrogen. Appendix A3 shows the table of the standard reduction potential of half-cell, the E_0 of hydrogen evolution by water which occurred at -0.83 V. Results found that the ΔE of the anhydrous methanol based electrolyte was 0.6177 V while the ΔE of contains deionized water was 0.76 V. Subsequently, the anodic and cathodic reactions shifted to the positive in the current densities. The polarization resistance and other properties were calculated using Butler-Volmer and Stern-Geary equations, as in Eqs. 2.6 and 2.7. Table 4.2 exhibits the electrochemical polarization parameters which consist of: corrosion potential (E_{corr}), corrosion current density (i_{corr}), anodic slope (β_a), cathodic slope (β_c) and polarization resistance (R_p).

Table 5.2 Results of Tafel polarization studies of aluminum in 3M KOH with anhydrous methanol, containing different amount of deionized water (0, 5, 10, 20)%wt.

Tafel polarization					
%Dionized water	E_{corr} (V vs Ag/AgCl)	i_{corr} (A cm ⁻²)	β_a (V dec ⁻¹)	β_c (V dec ⁻¹)	R_p (Ω)
0%water	-1.4	0.002	1.05	-6.18	252.31
5%water	-1.5	0.003	0.86	-5.50	119.04
10%water	-1.5	0.004	0.71	-4.88	61.11
20%water	-1.5	0.006	0.63	-3.60	36.71

According to Table 5.2, the corrosion potential (E_{corr}) indicated that the anodic process was much more affected than the cathodic process. The corrosion rate was related to the polarization resistance; higher polarization resistance exhibited lower corrosion current. Thereby, the higher polarization resistance indicated more corrosion inhibition property. The anodic slope (β_a) provided the corrosion tendency of the anode while the anodic Tafel slope meant how much overpotential was required in the reaction rate (Hosseini et al., 2018).

Resistance decreased when the amount of deionized water increased, respectively. The small slope indicating higher corrosion of aluminum occurred in the condition of 20%. The i_{corr} of the 20%water provided 0.006 A/cm^2 . The polarization resistance (R_p) was 36.71Ω which was the highest corrosion, but the lowest overpotential requirement. The highest anodic Tafel slope occurred in the anhydrous methanol based electrolyte. The i_{corr} of anhydrous provided 0.002 A/cm^2 while the polarization resistance was of 252.31Ω . Thus, the exhibition of aluminum corrosion proved to have a decisive advantage, but it required higher overpotential.

5.1.3 Electrochemical impedance spectroscopy (EIS)

EIS technique can predict the specific characteristic of the aluminum dissolution process as well as the behavior of corrosive aluminum. ZsimWin software was used to compute the equivalent circuit model according to each condition. The three-electrode cell was applied to the investigation. Frequencies in the EIS range were applied at 100k Hz-0.02 Hz; the frequencies were recorded and displayed as Nyquist plots.

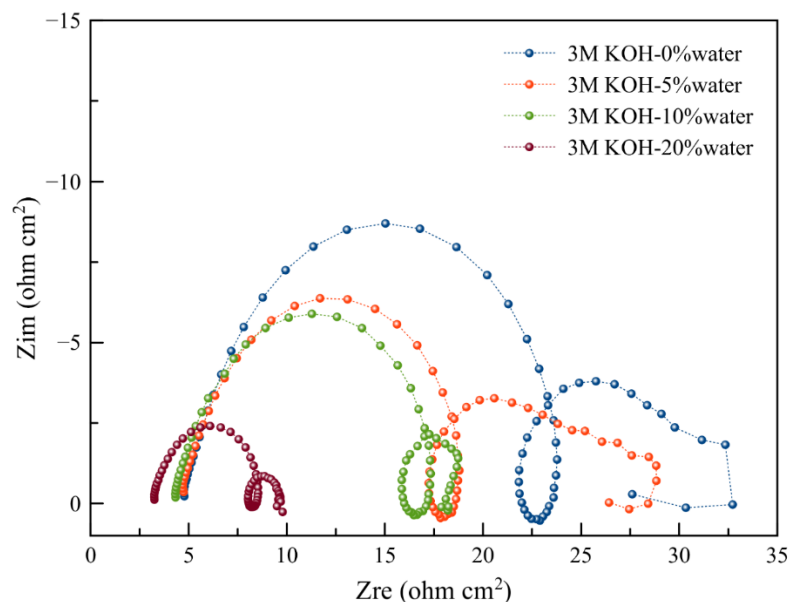


Figure 5.4 Nyquist plot of aluminum with anhydrous and contents of deionized water.

In Fig. 5.4 the impedance diagrams consist of semicircles. This means that the corrosion process is mainly charge transfer controlled (de Wit & Lenderink, 1996). The impedance

spectrum of aluminum in 3M-KOH mix solution with anhydrous, containing deionized water, consists of three loops: (i) a large capacitive loop at high frequency (ii) a small inductive loop at a middle frequency and (iii) a second small capacitive loop at a low frequency (Moghadam et al., 2017). The first capacitive semicircle at high frequencies is attributed to the redox reaction of $\text{Al} \leftrightarrow \text{Al}^+$. This was found to be the highest caused by charge transfer resistance in parallel with the double layer. Hence, it can be assumed to be the rate-determining step in the charge transfer process.

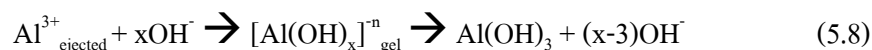
The small inductive loop at the middle frequencies was created by adsorbed intermediates on the aluminum surface. The adsorption of intermediate species such as $\text{Al}(\text{OH})_3$ and $\text{Al}(\text{OH})_4^-$ might be involved in the aluminum dissolution process (D. Wang et al., 2015). On the other hand, the second capacitive semicircle at low frequency is ascribed to the redox reaction of $\text{Al}^+ \leftrightarrow \text{Al}^{3+}$ which is the fast supplement step.

Another cause of this situation that occurred in the graph is that it related to double layer transition (Koroleva, Thompson, Hollrigl, & Bloeck, 1999). In their research, it was suggested that such a redox reaction may occur according to the process of an aluminum hydrous layer formation and subsequent precipitation of aluminum hydroxides.

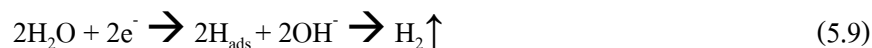
Anhydrous film; aluminum interface (anodic process):



Hydrous film; film/electrolyte interface (chemical process):



These reactions are accompanied by cathodic hydrogen evolution:



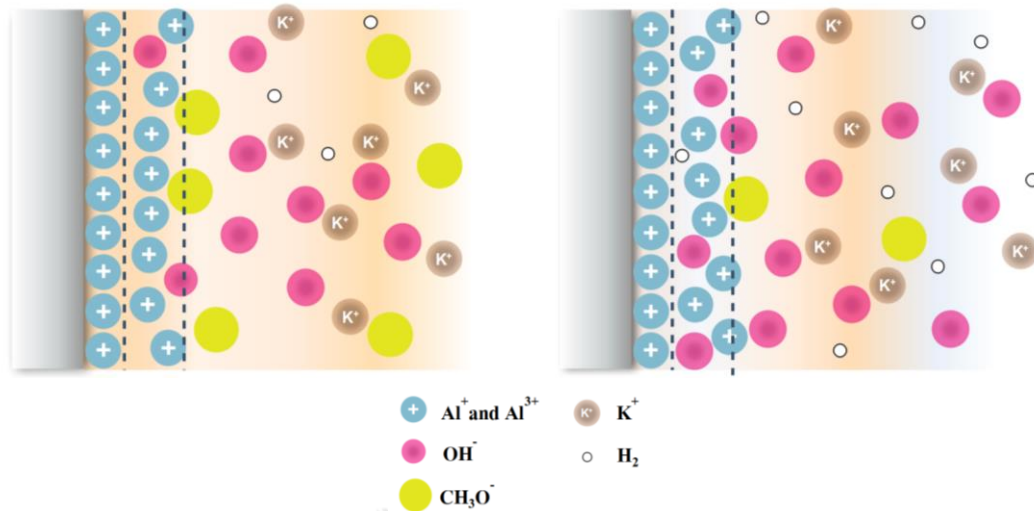


Figure. 5.5 prediction of aluminum's double layer in KOH based electrolyte with anhydrous and contents of deionized water.

Fig. 5.4 shows that the highest Nyquist plot diameter in the anhydrous methanol based electrolyte; the electrical double layer (EDL) was minimally consumed. Fig. 5.5 shows the prediction of the aluminum dissolution process that was related to EDL. As for the aluminum dissolution process, methyl oxide (CH₃O) may have helped to break the reaction between OH⁻ and Al³⁺ that was a main reactant which produced Al(OH)₃, Al(OH)₄⁻ or H₂. Yet, CH₃O⁻ did not react with the other substances. However, when the deionized water was increased, it led to a decrease in the diameter size of the capacitive semicircle because a higher amount of OH⁻ was produced. This meant that the increase in deionized water can decrease the charge-transfer resistance. However, the corrosion rate still increased. Moreover, the internal resistance related with the intercept at zero point of the real axis (Z_{re}). Thus, the lower internal resistance reached to negative shift. The EIS results indicated that the internal resistance of each condition shifted to negative when the deionized water percentage increased.

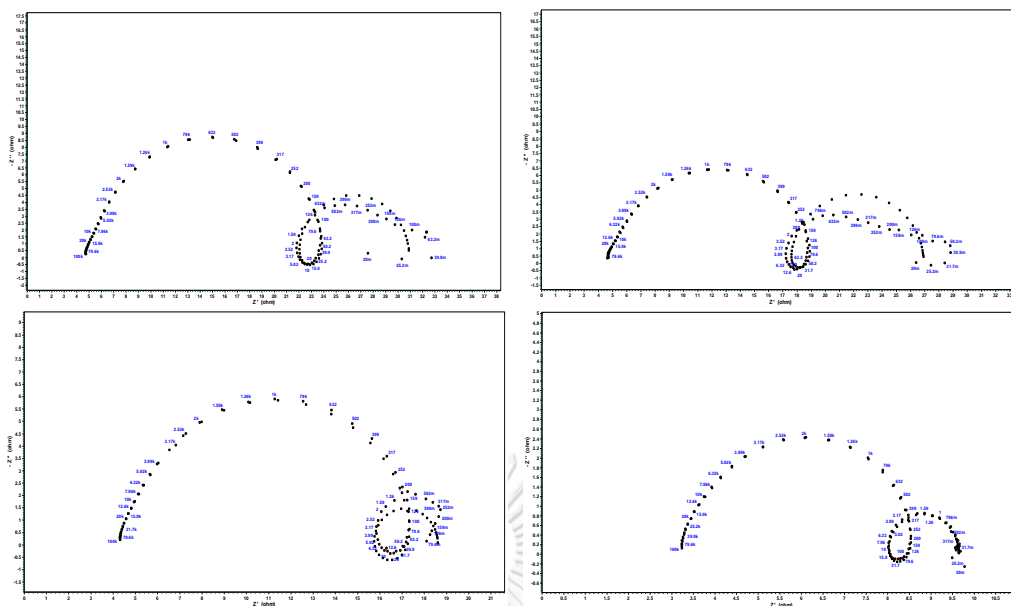


Figure 5.6 the experimental and computer fit results of Nyquist plot (1) 0% deionized water (2) 5% deionized water (3) 10% deionized water and (4) 20% deionized water.

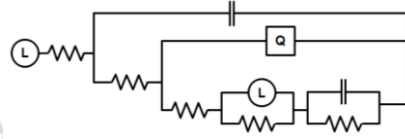


Figure 5.7 equivalent circuit fit aluminum in methanol 3M-KOH mix solution with anhydrous and content of deionized water.

Fig. 5.6 and Fig. 5.7 show the computer fit results of the Nyquist plots. ZsimWin software was used to compute the equivalent circuit model according to each condition. The equivalent circuit model as illustrated by Fig 5.7, includes the solution resistance (R_s) series with the inductor (L), a capacitor (C_1) in parallel to the series of CPE (Q) and capacitor (C_2) and series resistors R_1 , R_2 , R_L , R_3 . R_L is parallel with the inductor L . The charge-transfer resistance (R_c) was calculated from this equation:

$$R_c = R_1 + R_2 + R_3 + R_L \quad (\text{Eq. 5.1})$$

Table 5.3 Results of EIS studies of aluminum in methanol 3M KOH mixed solution

%Deionized water	EIS parameters							
	Rs (Ω/cm^2)	CPE	R1 (Ω/cm^2)	R2 (Ω/cm^2)	RL (Ω/cm^2)	CPE2	R3 (Ω/cm^2)	Rp (Ω/cm^2)
0%water	2.233	19.380	39.760	13.050	18.780	6.821	3.065	74.66
5%water	1.458	12.190	34.230	16.720	12.730	18.940	7.648	49.228
10%water	1.227	10.160	23.260	6.684	11.900	7.181	3.160	45.004
20%water	0.380	3.402	8.821	9.939	5.066	4.148	1.594	20.354

Table 5.3 shows the computer fitting results of the Nyquist plots for aluminum in methanol-KOH mixed solution with different contents of deionized water. The ZsimWin program was used to calculate the charge-transfer resistance. The results indicated that the internal resistance (R_s) of the aluminum dissolution process significantly decreased. This indicated that the deionized water acted in line with the catalyst and helped to decrease the double layer of aluminum in the dissolution process.

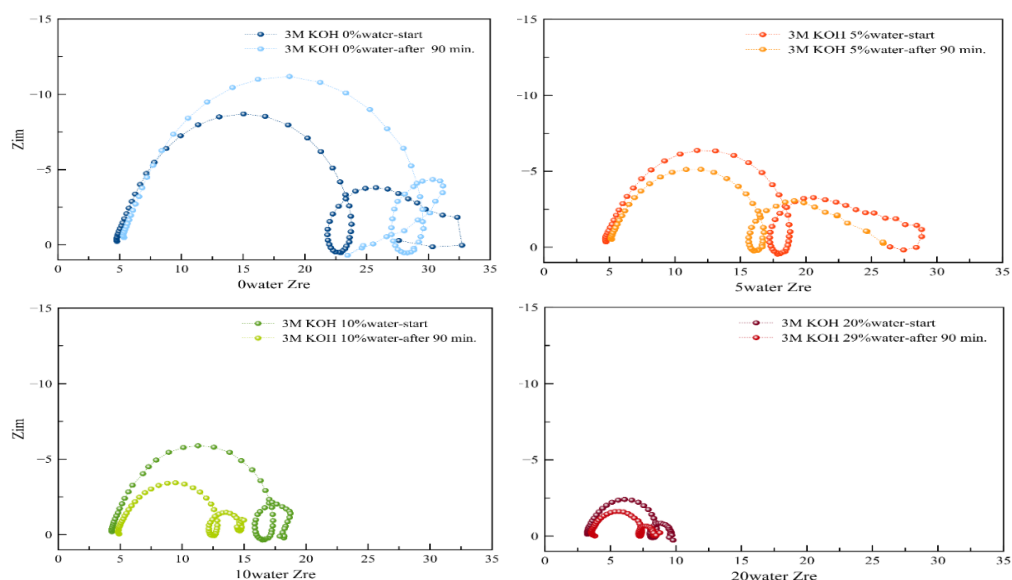


Figure 5.8 comparison of aluminum at immediate immersion and after Tafel polarization test for 90 min. for each condition (1) 0%water (2) 5%water (3) 10%water and (4) 20%water.

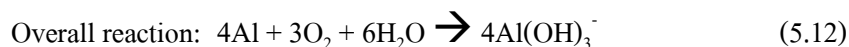
Fig 5.8 shows the impedance diagrams at immediate immersion of aluminum and after discharging 90 min. Thus, it was found that only the anhydrous methanol based electrolyte increased its diameter as regards the capacitive and inductive loops more than before. It may be higher because of the slow reaction of methyl oxide (CH_3O^-). In another case, where the deionized water was varied, the width of the capacitive semicircle decreased due to aluminum corrosion caused by the aluminum dissolution process.

5.2 Battery performance

Following the half-cell studies, the characteristic of the aluminum dissolution process in the electrolyte can be predicted by using EIS technique as well as Tafel polarization. This section aims to study battery performance containing different percentages of deionized water. The dual-electrolyte system was used in this investigation and improved battery performance.

5.2.1 Effect of deionized water in the polarization of the I-V curve and power density

In Figs. 5.9 and 5.10, the polarization of the I-V curves and power density are shown; providing the best supporting data. The standard form of Al-air battery depends on the type of electrolyte that participates in the reaction. The electrochemical reaction at the electrodes hydroxide base can be signified as follows (Mokhtar et al., 2015):



Aluminum also has a parasitic reaction to hydrogen evolution:



Figs. 5.9 and 5.10 shows the polarization curves and power density plots of the aluminum-air battery. The limiting current density for each condition slightly increased as follows: 14.97 mA/cm^2 , 17.50 mA/cm^2 , 30 mA/cm^2 and 36.3 mA/cm^2 at 0%water, 5%water, 10%water and 20%water respectively. The maximum power density was calculated via current

density and voltage providing: 4.78 mW/cm², 8.41 mW/cm², 15.45 mW/cm² and 19.60 mW/cm² respectively.

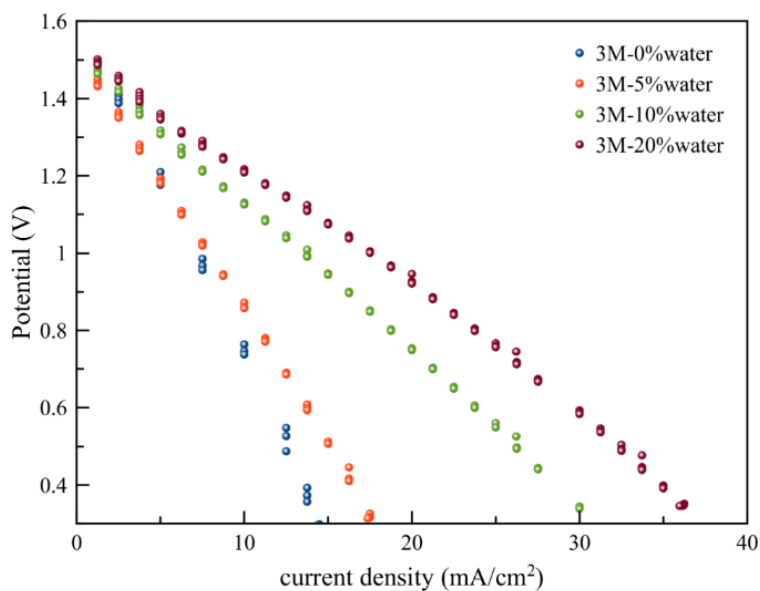


Figure 5.9 polarization curves of the aluminum-air battery with dual-electrolyte.

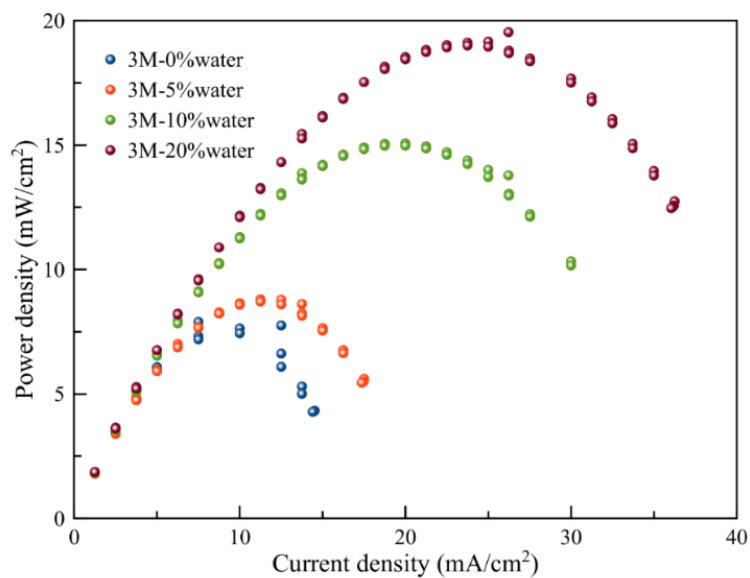


Figure 5.10 power density plots of the aluminum-air flow battery using dual-electrolyte system with anhydrous methanol based electrolyte and deionized water.

As seen in Appendix A2, the internal resistance can be calculated. The internal resistance provided: 76.7 Ω , 65.7 Ω , 39.24 Ω and 33.09 Ω respectively. All the results show that the

internal resistance was high because the pathway from the anode to cathode electrodes was wide, including the anion exchange membrane (L. Wang et al., 2014). The supply of deionized water improved their electrical performance because of its activity in line with that of a catalyst, thereby promoting reaction and producing much more aluminum hydroxide ions ($\text{Al}(\text{OH})_3^-$). The deionized water leads to low internal resistance and faster reaction between aluminum and air at the cathode, according to the EISs results; namely that R_s was related to the internal resistance of the aluminum dissolution process. When the deionized water percentage was raised, the internal resistance significantly decreased. This may be due to the decrease in the double layer of the aluminum surface. Subsequently, there was a decrease in viscosity which promoted the mass transfer.

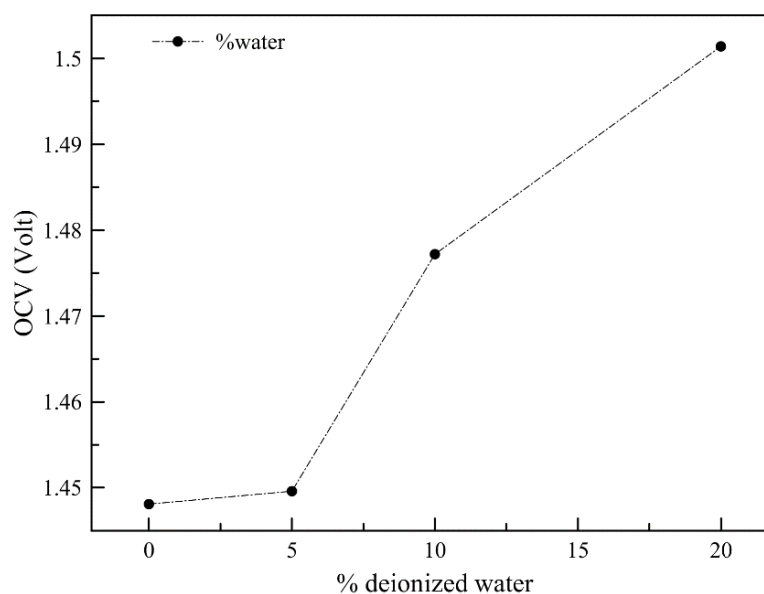


Figure 5.11 the comparison of OCVs between various deionized water

The results exhibit linear polarization curves with OCVs for the condition (0, 5, 10, and 20)%water. The OCV of the anhydrous methanol based electrolyte provided 1.4481 V. Thus, when the deionized water was increased, the OCVs provided: 1.4496 V, 1.4772 V, and 1.5014 V respectively. It is evident that by increasing the deionized water OCV improved, but it produced a higher hydrogen evolution rate. Table 5.4 includes the maximum current density, OCVs, power density and internal resistance of the aluminum-air battery.

Table 5.4 shows the maximum current density, OCVs, power density and internal resistance of the aluminum-air battery

% deionized water	OCV (V)	limiting current density (mA/cm ²)	Maximum power density (mW/cm ²)	Internal resistance (Ω)
0%water	1.4481	14.7	4.78	76.7
5%water	1.4496	17.5	8.41	65.7
10%water	1.4772	30	15.45	39.24
20%water	1.5014	36.3	19.60	33.09

5.2.2 Effect of deionized water in discharge profile

Full battery discharge profiles were performed with anhydrous and contained different percentages of deionized water based on methanol 3M-KOH solution. One hour before testing, the anion membrane was put in the system between the anolyte and catholyte. In Fig. 5.12, the discharge profile is presented, and the battery was discharged at the rate of 10 mA/cm². Table 5.5 summarizes each condition: specific capacity, utilization percentage and the lifetime of each condition. As a result, aluminum was consumed until the substance was exhausted.

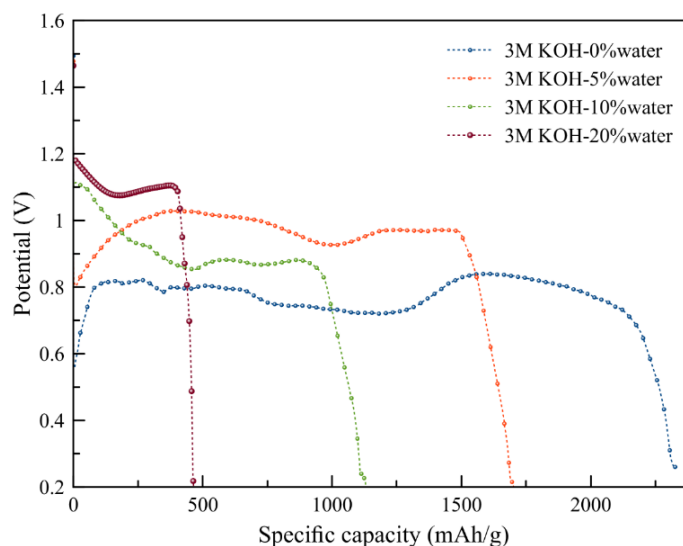


Figure 5.12 capacity density of aluminum in aluminum-air flow battery using dual-electrolyte system with anhydrous methanol based electrolyte and deionized water at discharging 10 mA/cm².

As observed, the discharging at 10 mA/cm^2 was a specific characteristic that fluctuated throughout the time frame. This spectacle occurs when a battery discharges close to maximum power density. The 0%water and 5%water had a current density of 14.7 mA/cm^2 and 17.5 mA/cm^2 that was sensitive due to many factors, such as gas bubble or the reaction in the air cathode. At the beginning, the discharge rapidly dropped until a minimum was reached and the voltage recovered slightly. Next, after the initial dip, the voltage remained almost constant. Then, the voltage gradually changed for a second time. This feature occurred at the same time of the discharge, regardless of the current. Finally, the voltage decreased until it reached the cut-off voltage for the remaining period. This same problem was found in an ionic liquid electrolyte because of the reaction in the air cathode, as suggested in the literature (D. Gelman et al., 2014). Stamm, Varzi, Latz, & Horstmann (2017) also have suggested that the initial drop in voltage is due to slow oxygen reduction which can lead to an abrupt voltage drop from the OCV. According to this, it may be possible because the MnO_2 as the catalyst at the air cathode electrode was not a perfect catalyst.

As for the condition of 10%water and 20%water, both were investigated, but the voltage did not drop as happened previously with the condition of 0%water and 5%water. Hence, the investigation did not proceed due to the discharge being far removed from maximum power density. Thus, the reaction of the cathode can be assumed to be the rate remitting step; specific capacity was not affected.

Table 5.5 summary of specific capacity, utilization percentage and lifetime of battery discharging at 10 mA/cm^2 .

% deionized water	Specific capacity (mAh/g)	Utilization percentage (Approximate)	Life time (hours)	Average voltage (V)
0%water	2328	78%	~40	0.757
5%water	1700	57%	~28	0.914
10%water	1130	38%	~18	0.9111
20%water	465	16%	~7	1.061

In the discharging profile, it can be seen that the anhydrous methanol based electrolyte achieved a specific capacity of 2328 mAh/g for around 40 hrs. This proved to be the highest capacity showing that aluminum could exhibit a significant higher coulombic efficiency in the anhydrous methanol based electrolyte. Accordingly, the hydrogen evolution rate was around 0.017 ml/cm² min., that was the lowest, emphasizing the fact that the parasitic reaction was almost completely suppressed. It is a fact that aluminum can be consumed more than 75% at an average voltage of 0.757 V. When the deionized water was increased, the specific capacity decreased consecutively: from 1700 mAh/g, 1130 mAh/g and 465 mAh/g at the condition of (5, 10, and 20)%water, respectively. Simultaneously, when the deionized water was increased, average voltage also increased, but utilization percentage decreased. Thus, it was found that the condition of 5%water can improve average voltage more than 0.2 V and can provide utilization percentage of around 57% for 28 hours. The condition of 10%water had a lower average voltage, due to the faster reaction of aluminum, in line with the condition of 20%water. In methanol-KOH solution, corrosive aluminum is significantly inhibited, but corrosion in the battery substantially increased when percentage of water increased. However, battery performance still provided a specific capacity of more than 50% at the condition of 5%water.

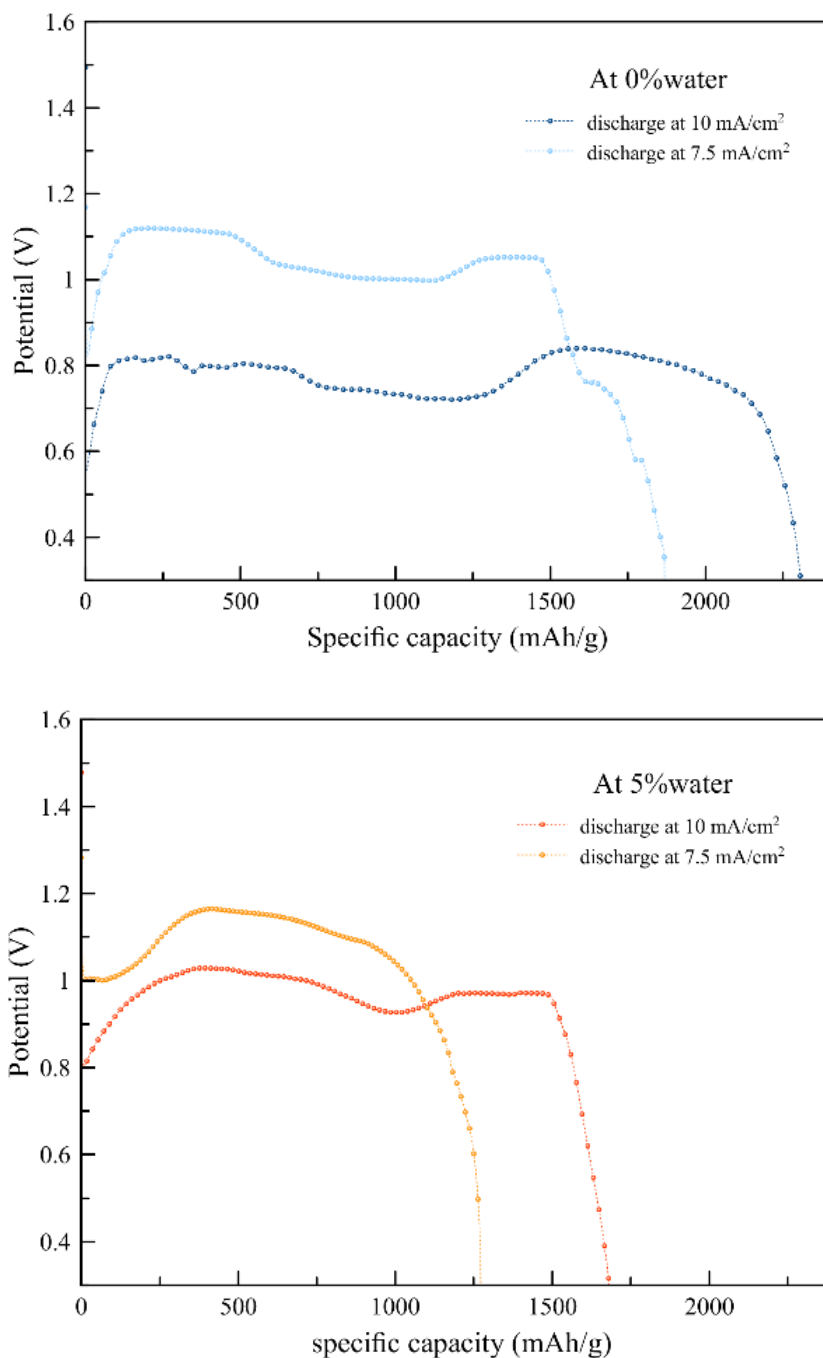


Figure 5.13 different discharging at 10 mA/cm² and 7.5 mA/cm² of 0%water and 5%water.

The discharge profiles, as shown in Fig. 5.13, illustrate the aluminum-air battery. For both conditions, the results indicated that the average voltage at 7.5 mA/cm² was higher than 10 mA/cm². For the condition 0%water and 5%water, the average voltages were 0.970 V and 1.056 V, respectively but specific capacity significantly decreased by around 15%. Fig. 5.14 shows the

potential and lifetime of the battery at different discharging times. It is observed that both of them finished almost the same time. This is because the two reactions, aluminum-air reaction and parasitic reaction, occurred at the same time, as indicated in Eqs. 4.10-4.13. The parasitic reaction not only pilfered electrons to generate hydrogen but also released electrons to the external circuit; specific capacity decreased with discharge at 7.5 mA/cm^2 .

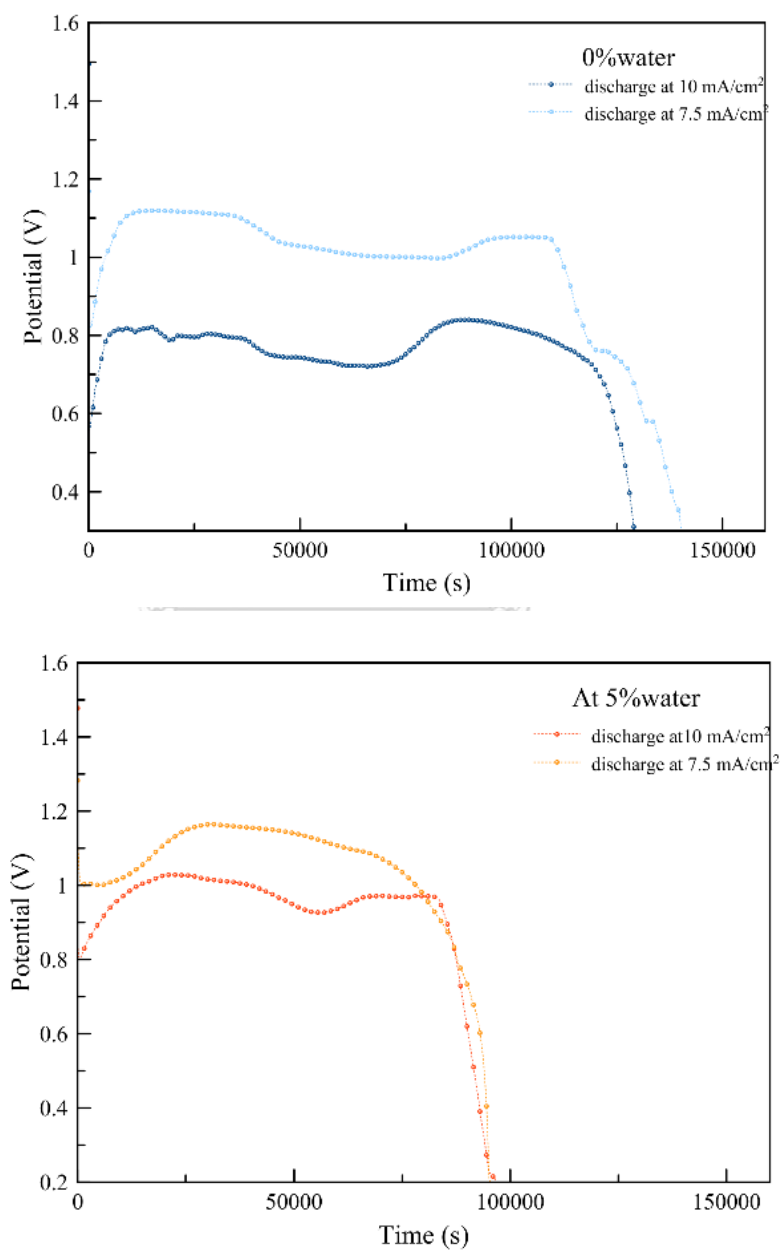


Figure 5.14 discharge times with different discharge at 7.5 mA/cm^2 and 10 mA/cm^2 .

5.2.3 Effect of flow rate with anhydrous methanol based electrolyte

The battery of the condition 0%water was investigated by employing different flow rates i.e. 20rpm (85 ml/min), 40rpm (160 ml/min) and 60rpm (240 ml/min). Fig. 5.15 shows the different flow rates of anolyte when discharging at 10 mA/cm^2 . As a result, aluminum was used up until finished, in line with the previous experiment.

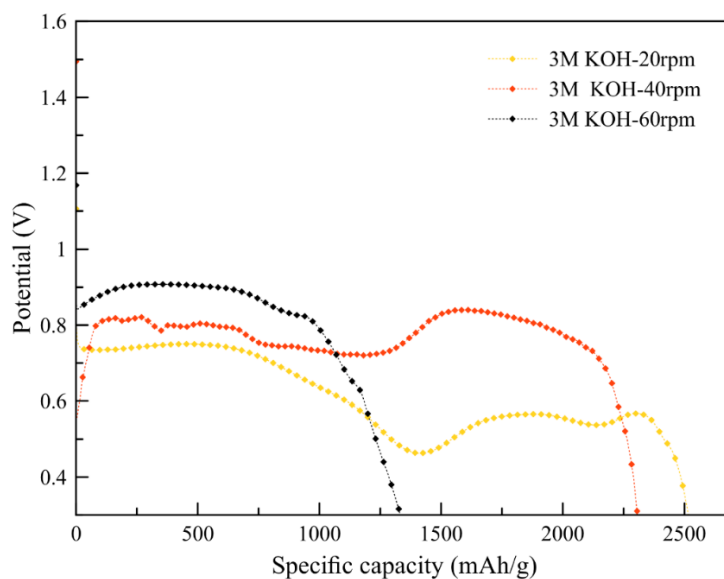


Figure 5.15 discharge profile of anhydrous methanol based electrolyte with different flow rates: 20rpm, 40rpm and 60rpm.

Table 5.6 summary of the discharging profile of anhydrous methanol based electrolyte with different flow rates.

Flow rate	Average voltage	Specific capacity	Percentage utilization
20rpm	0.605	2500	84%
40rpm	0.757	2328	78%
60rpm	0.772	1350	45%

Fig 5.15 indicates that the highest specific capacity occurred at 20rpm, while the average voltage was 0.605 V. According to the research, J.-B. Wang et al (2007) suggested that aluminum passivation will appear after discharging around 4-5 hours with aluminum in methanol-KOH solution. This research also provided discharging times less than 20 hours because of the aluminum's passivation, which was lower than using flow electrolyte. At 20rpm, the average voltage was low because the continuous flow rate was very slow due to passivation. However, at 40rpm, specific capacity dropped slightly. At 60rpm, specific capacity dropped significantly. The higher flow rate brought about the consumption of the aluminum. This led to the short lifetime of the battery.



Chapter 6

Conclusions

In this research, the studies were classified into two sections: half-cell and full-cell batteries. In the case of half-cell, the mechanism of the aluminum dissolution process and the behavior of corrosive aluminum, in methanol-KOH based electrolyte with different percentages of deionized water, were investigated. Hydrogen evolution, Tafel polarization and EIS technique were applied. The result of hydrogen evolution with aluminum immersing at 90 min. presented an increase in the loss of aluminum weight when the hydrogen gas volume increased, following the increase in water percentage. This was due to self-corrosion of the aluminum. The behavior of aluminum, as operated by the Tafel polarization at potential 0.5 mV/s, expressed much overpotential required in anhydrous methanol based electrolyte and highest polarization resistance. Both behaviors can be reduced by increasing the deionized water, but the self-corrosion of aluminum is of concern. As for the EIS technique, charge-transfer resistance, as calculated by a fitting model, indicated a small decrease in aluminum protective oxide film. As mentioned, the tendency of results are similar because aluminum can be produced in three ways providing: aluminum protective oxide film, parasitic reaction and aluminum ion ($\text{Al}(\text{OH})_4^-$). In addition, water in the methanol based electrolyte acted as a catalyst to produce much of the $\text{Al}(\text{OH})_3^-$ resulting in faster reaction. It also had other effects on the electrolyte as follows: decreasing aluminum double-layer, increasing mass transfer owing to the decrease in electrolyte viscosity and enhancing conductivity. However, increasing deionized water caused considerable more hydrogen gas which was related to self-corrosion.

For the full-cell battery, its anhydrous methanol based electrolyte was varied employing different water percentages. The dual-electrolyte system completely suppressed the parasitic reaction and provided the highest specific capacity of 2,328 mAh/g discharging at 10 mA/cm². The aluminum consumption had more than 75%. In addition, the performance of the aluminum-air battery increased when the electrolyte contained water less than 5%. The condition 5%water can improve average voltage with minimal loss of specific capacity from the self-corrosive

aluminum. Besides, the different flow rates of electrolyte were examined. The results indicated that increasing flow rates provided higher average voltage because the passivation was cleared on the aluminum surface.



Appendix

In the following additional information, equations for the experiment in this thesis are given.

A1. Hydrogen evolution rate equation (D. Wang et al., 2015):

$$R_h = \frac{V}{A \times T}$$

where R_h is hydrogen evolution rate (ml/cm²min), A is specimen area (cm²), V is the volume of hydrogen gas collected (ml) and T is the immersion period (min).

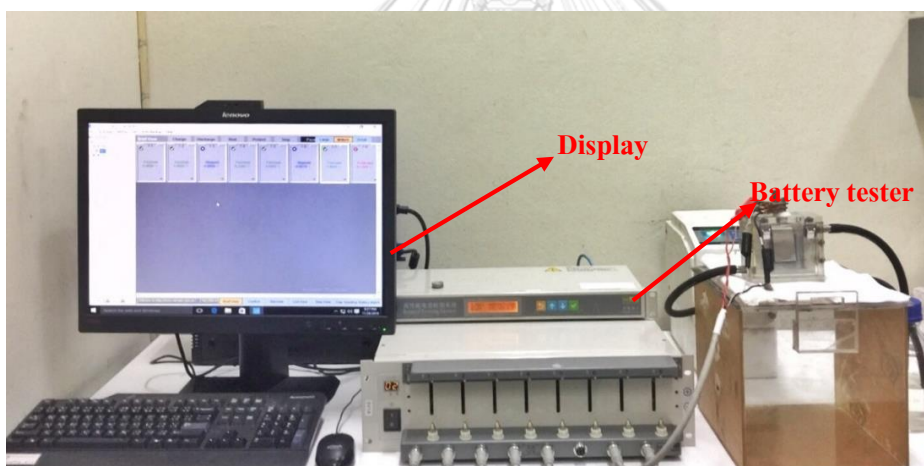
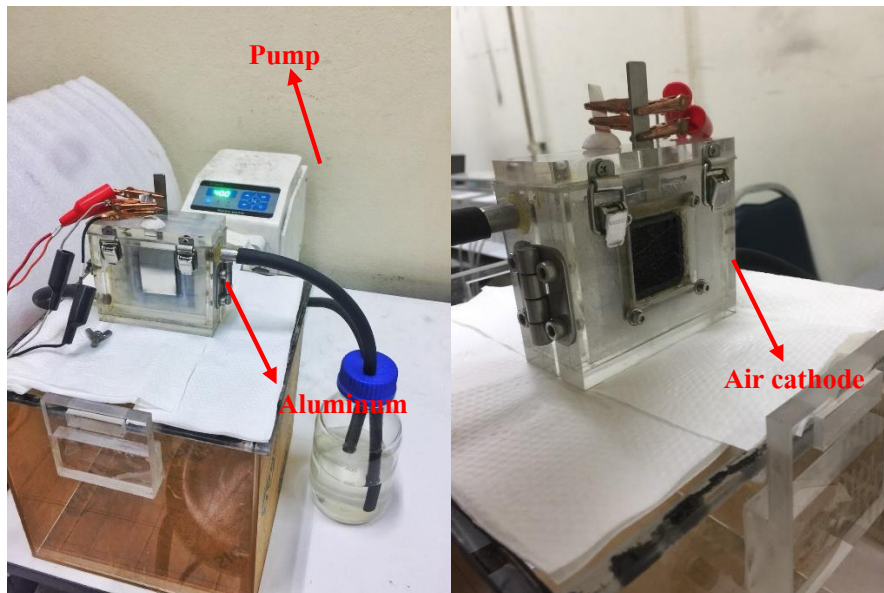
A2. The internal resistance of battery

$$R_{internal} = \frac{\Delta V}{\Delta I}$$

where $R_{internal}$ is internal resistance of battery (Ω), ΔV is the different voltage between the OCV and voltage at the limiting current density point and ΔI is the different current between the limiting current and starting current.

A3. The standard reduction potentials (Harris, 2011)

Material	reaction	E° (volts)
Aluminum	$Al^{3+} + 3e^- \leftrightarrow Al(s)$	-1.677
	$Al(OH)_4^- + 3e^- \leftrightarrow Al(s) + 4OH^-$	-2.328
Oxygen	$O_2 + 2H_2O + 4e^- \rightarrow 4OH^-$	0.3
Hydrogen	$H_2O + e^- \leftrightarrow 1/2H_2(g) + OH^-$	-0.828

A4. The operation of cell experiment of aluminum-air battery with flow anolyte system

REFERENCES



จุฬาลงกรณ์มหาวิทยาลัย
CHULALONGKORN UNIVERSITY

- Abdel-Gawad, S. A., Osman, W. M., & Fekry, A. M. (2018). Characterization and Corrosion behavior of anodized Aluminum alloys for military industries applications in artificial seawater. *Surfaces and Interfaces*.
- Chaubey, N., Yadav, D. K., Singh, V. K., & Quraishi, M. A. (2017). A comparative study of leaves extracts for corrosion inhibition effect on aluminium alloy in alkaline medium. *Ain Shams Engineering Journal*, 8(4), 673-682.
- Chen, B., Leung, D. Y. C., Xuan, J., & Wang, H. (2017). A mixed-pH dual-electrolyte microfluidic aluminum–air cell with high performance. *Applied Energy*, 185, 1303-1308.
- Chen, B., Xuan, J., Wang, H., & Leung, D. Y. C. (2017). Microfluidic Aluminum-air Cell with Methanol-based Anolyte. *Energy Procedia*, 105, 4691-4697.
- Cho, Y.-J., Park, I.-J., Lee, H.-J., & Kim, J.-G. (2015). Aluminum anode for aluminum–air battery – Part I: Influence of aluminum purity. *Journal of Power Sources*, 277, 370-378.
- de Wit, J. H. W., & Lenderink, H. J. W. (1996). Electrochemical impedance spectroscopy as a tool to obtain mechanistic information on the passive behaviour of aluminium. *Electrochimica Acta*, 41(7), 1111-1119.
- Deepa, P., & Padmalatha, R. (2017). Corrosion behaviour of 6063 aluminium alloy in acidic and in alkaline media. *Arabian Journal of Chemistry*, 10, S2234-S2244.
- Di Palma, T. M., Migliardini, F., Caputo, D., & Corbo, P. (2017). Xanthan and κ-carrageenan based alkaline hydrogels as electrolytes for Al/air batteries. *Carbohydrate Polymers*, 157, 122-127.
- Digne, M., Sautet, P., Raybaud, P., Toulhoat, H., & Artacho, E. (2002). Structure and Stability of Aluminum Hydroxides: A Theoretical Study. *The Journal of Physical Chemistry B*, 106(20), 5155-5162.
- Egan, D. R., Ponce de León, C., Wood, R. J. K., Jones, R. L., Stokes, K. R., & Walsh, F. C. (2013). Developments in electrode materials and electrolytes for aluminium–air batteries. *Journal of Power Sources*, 236, 293-310.
- Fan, L., & Lu, H. (2015). The effect of grain size on aluminum anodes for Al–air batteries in alkaline electrolytes. *Journal of Power Sources*, 284, 409-415.
- Fan, L., Lu, H., & Leng, J. (2015). Performance of fine structured aluminum anodes in neutral and alkaline electrolytes for Al-air batteries. *Electrochimica Acta*, 165, 22-28.
- Fan, L., Lu, H., Leng, J., Sun, Z., & Chen, C. (2015). The effect of crystal orientation on the aluminum anodes of the aluminum–air batteries in alkaline electrolytes. *Journal of Power Sources*, 299, 66-69.
- Frankel, G. S. (2016). Fundamentals of Corrosion Kinetics. In A. E. Hughes, J. M. C. Mol, M. L. Zheludkevich, & R. G. Buchheit (Eds.), *Active Protective Coatings: New-Generation Coatings for Metals* (pp. 17-32). Dordrecht: Springer Netherlands.
- Gelman, D., Lasman, I., Elfimchev, S., Starosvetsky, D., & Ein-Eli, Y. (2015). Aluminum corrosion mitigation in alkaline electrolytes containing hybrid inorganic/organic inhibitor system for power sources applications. *Journal of Power Sources*, 285, 100-108.
- Gelman, D., Shvartsev, B., & Ein-Eli, Y. (2014). Aluminum–air battery based on an ionic liquid electrolyte. *Journal of Materials Chemistry A*, 2(47), 20237-20242.
doi:10.1039/C4TA04721D
- Hagesteijn, K. F. L., Jiang, S., & Ladewig, B. P. (2018). A review of the synthesis and characterization of anion exchange membranes. *Journal of Materials Science*, 53(16), 11131-11150.

- Han, B., & Liang, G. (2006). Neutral electrolyte aluminum air battery with open configuration. *Rare Metals*, 25(6, Supplement 1), 360-363.
- Han, X., Qu, Y., Dong, Y., Zhao, J., Jia, L., Yu, Y., . . . Feng, Y. (2018). Microbial electrolysis cell powered by an aluminum-air battery for hydrogen generation, in-situ coagulant production and wastewater treatment. *International Journal of Hydrogen Energy*, 43(16), 7764-7772.
- Harris, D. C. (2011). *Solutions manual for Harris' Quantitative chemical analysis, eighth edition*: New York, NY : W.H. Freeman and Co., [2011] ©2011.
- Hopkins, B. J., Shao-Horn, Y., & Hart, D. P. (2018). Suppressing corrosion in primary aluminum–air batteries via oil displacement. *Science*, 362(6415), 658-661.
- Hosseini, S., Lao-Atiman, W., Han, S. J., Arpornwichanop, A., Yonezawa, T., & Kheawhom, S. (2018). Discharge Performance of Zinc-Air Flow Batteries Under the Effects of Sodium Dodecyl Sulfate and Pluronic F-127. *Scientific reports*, 8(1), 14909-14909.
- Koroleva, E. v., Thompson, G. e., Hollrigl, G., & Bloeck, M. (1999). Surface morphological changes of aluminium alloys in alkaline solution:: effect of second phase material. *Corrosion Science*, 41(8), 1475-1495.
- Kruehong, C. Performance of Aluminum-Air Battery in Mixed Solutions between NaOH and NaCl. In.
- Levy, N. R., Auinat, M., & Ein-Eli, Y. (2018). Tetra-butyl ammonium fluoride – An advanced activator of aluminum surfaces in organic electrolytes for aluminum-air batteries. *Energy Storage Materials*, 15, 465-474.
- Li, L., & Manthiram, A. (2013). Dual-electrolyte lithium–air batteries: influence of catalyst, temperature, and solid-electrolyte conductivity on the efficiency and power density. *Journal of Materials Chemistry A*, 1(16), 5121-5127.
- Li, L., Zhao, X., & Manthiram, A. (2012). A dual-electrolyte rechargeable Li-air battery with phosphate buffer catholyte. *Electrochemistry Communications*, 14(1), 78-81.
- Li, Q., & Bjerrum, N. J. (2002). Aluminum as anode for energy storage and conversion: a review. *Journal of Power Sources*, 110(1), 1-10.
- Liu, Y., Sun, Q., Li, W., Adair, K. R., Li, J., & Sun, X. (2017a). A comprehensive review on recent progress in aluminum–air batteries. *Green Energy & Environment*, 2(3), 246-277.
- Liu, Y., Sun, Q., Li, W., Adair, K. R., Li, J., & Sun, X. (2017b). A comprehensive review on recent progress in aluminum–air batteries. *Green Energy & Environment*.
- Ma, J., Wen, J., Gao, J., & Li, Q. (2014). Performance of Al–0.5 Mg–0.02 Ga–0.1 Sn–0.5 Mn as anode for Al–air battery in NaCl solutions. *Journal of Power Sources*, 253, 419-423.
- Modestino, M. A., Hashemi, S. M. H., & Haussener, S. (2016). Mass transport aspects of electrochemical solar-hydrogen generation. *Energy & Environmental Science*, 9(5), 1533-1551.
- Moghadam, Z., Shabani-Nooshabadi, M., & Behpour, M. (2017). Electrochemical performance of aluminium alloy in strong alkaline media by urea and thiourea as inhibitor for aluminium-air batteries. *Journal of Molecular Liquids*, 242, 971-978.
- Mokhtar, M., Talib, M. Z. M., Majlan, E. H., Tasirin, S. M., Ramli, W. M. F. W., Daud, W. R. W., & Sahari, J. (2015). Recent developments in materials for aluminum–air batteries: A review. *Journal of Industrial and Engineering Chemistry*, 32, 1-20.
- Mori, R. (2014). A novel aluminium–air secondary battery with long-term stability. *RSC Advances*, 4(4), 1982-1987.
- Mori, R. (2015). Capacity recovery of aluminium–air battery by refilling salty water with cell structure modification. *Journal of Applied Electrochemistry*, 45(8), 821-829.

- Mori, R. (2017). Electrochemical properties of a rechargeable aluminum–air battery with a metal–organic framework as air cathode material. *RSC Advances*, 7(11), 6389–6395.
- Mukherjee, A., & Basumallick, I. N. (1996). Complex behaviour of aluminium dissolution in alkaline aqueous 2-propanol solution. *Journal of Power Sources*, 58(2), 183–187.
- Mutlu, R. N., & Yazıcı, B. (2018). Copper-deposited aluminum anode for aluminum-air battery. *Journal of Solid State Electrochemistry*.
- Santos., D. M. F., & Sequeira., C. A. C. (2013). HYDROGEN PRODUCTION BY ALKALINE WATER ELECTROLYSIS. *Quim. Nova*, 36, 1176–1193.
- Shvartsev, B., Gelman, D., Amram, D., & Ein-Eli, Y. (2015). Phenomenological Transition of an Aluminum Surface in an Ionic Liquid and Its Beneficial Implementation in Batteries. *Langmuir*, 31(51), 13860–13866.
- Stamm, J., Varzi, A., Latz, A., & Horstmann, B. (2017). Modeling nucleation and growth of zinc oxide during discharge of primary zinc-air batteries. *Journal of Power Sources*, 360, 136–149.
- Takashi Hibino, Kobayashi, K., & Nagao, M. (2013). An all-solid-state rechargeable aluminum–air battery with a hydroxide ion-conducting Sb(V)-doped SnP2O7 electrolyte. *Journal of Materials Chemistry A*, 1, 14844–14848. doi:10.1039/c3ta12707a
- Tang, Y., Lu, L., Roesky, H. W., Wang, L., & Huang, B. (2004). The effect of zinc on the aluminum anode of the aluminum–air battery. *Journal of Power Sources*, 138(1), 313–318.
- Wang, D., Li, H., Liu, J., Zhang, D., Gao, L., & Tong, L. (2015). Evaluation of AA5052 alloy anode in alkaline electrolyte with organic rare-earth complex additives for aluminium-air batteries. *Journal of Power Sources*, 293, 484–491.
- Wang, J.-B., Wang, J.-M., Shao, H.-B., Zhang, J.-Q., & Cao, C.-N. (2007). The corrosion and electrochemical behaviour of pure aluminium in alkaline methanol solutions. *Journal of Applied Electrochemistry*, 37(6), 753–758.
- Wang, J. B., Wang, J. M., Shao, H. B., Chang, X. T., Wang, L., Zhang, J. Q., & Cao, C. N. (2009). The corrosion and electrochemical behavior of pure aluminum in additive-containing alkaline methanol–water mixed solutions. *Materials and Corrosion*, 60(4), 269–273.
- Wang, L., Liu, F., Wang, W., Yang, G., Zheng, D., Wu, Z., & Leung, M. K. H. (2014). A high-capacity dual-electrolyte aluminum/air electrochemical cell. *RSC Advances*, 4(58), 30857–30863.
- Zhang, Z., Zuo, C., Liu, Z., Yu, Y., Zuo, Y., & Song, Y. (2014). All-solid-state Al–air batteries with polymer alkaline gel electrolyte. *Journal of Power Sources*, 251, 470–475.
- Zhuk, A. Z., Kleimenov, B. V., Udaltsov, V. G., Kiseleva, E. A., & Tarasenko, A. B. (2018). An Electrochemical Generator Containing Cylindrical Aluminum-Air Cells. *Thermal Engineering*, 65(7), 420–428.

VITA

NAME Pemika Teabnamang

DATE OF BIRTH 01 January 1994

PLACE OF BIRTH Nakhonsawan, Thailand

INSTITUTIONS ATTENDED Bachelor's in Chemical engineering, Khonkaen, Thailand

HOME ADDRESS 9 Chongkhae pattana, Chongkhae, Takli, Nakhon sawan

